VEHICLE-TO-VEHICLE COMMUNICATIONS FOR INTELLIGENT VEHICLE HIGHWAY SYSTEMS

by

Tushar Tank

Memorandum No. UCB/ERL M94/85

17 October 1994

VEHICLE-TO-VEHICLE COMMUNICATIONS FOR INTELLIGENT VEHICLE HIGHWAY SYSTEMS

by

Tushar Tank

Memorandum No. UCB/ERL M94/85

17 October 1994

ELECTRONICS RESEARCH LABORATORY

College of Engineering
University of California, Berkeley
94720

VEHICLE-TO-VEHICLE COMMUNICATIONS FOR INTELLIGENT VEHICLE HIGHWAY SYSTEMS

by

Tushar Tank

Memorandum No. UCB/ERL M94/85

17 October 1994

ELECTRONICS RESEARCH LABORATORY

College of Engineering
University of California, Berkeley
94720

Vehicle-to-Vehicle Communications For Intelligent Vehicle Highway Systems

Tushar Tank

Department of Electrical Engineering
and Computer Science
University of California at Berkeley
Berkeley, California 94720

Abstract

Vehicle-to-vehicle radio links suffer from power variations, multipath fading and associated Doppler spreading in frequency, as well as interference form other vehicles. We discuss the impact of these effects on communication networks supporting an Intelligent Vehicle Highway System (IVHS). A statistical model for this channel is considered and the performance of the network involving many links is evaluated. We compare the performance of Time Division Multiple Access (TDMA), Direct Sequence Code Division Multiple Access (DS-CDMA), and Frequency Hopping with TDMA in this environment. Reliability of the radio link is investigated by specifying the radio spectrum occupation for a given required reliability of the radio link.

Acknowledgments

I am deeply indebted to my parents for their support and encouragement over the last two years. I would also like to thank Professor Jean-Paul Linnartz, without whose ideas and discussions this report would not have been possible. To my friends back on the east coast, whose summer visit and email conversions have kept me sane, my sister, who did not bother me for the most part, and my peers in Room 307, who have given a new meaning to the word diversion, I also extend my gratitude. And finally I would like to thank my extended family at the Bochasanwasi Shri Akshar Purshottom Swaminarayan Temple in Milpitas for their support.

Table of Contents

Introduction

1.0 Introduction

Recently implementation of advance communication technology has been propounded as a feasible alternative to solving ground transportation problems. Projects such as Road Automobile Communication Systems (RACS) in Japan [1], PROMETHEUS in Europe [2], and Partners for Advanced Transit and Highway (PATH) in the U.S. are currently engaged in the design of such systems called Intelligent Vehicle Highway Systems (IVHS) in Japan and the United States and Road Transport Informatics (RTI) in Europe. These projects encompass Automated Vehicle Control Systems (AVCS), Advanced Traffic Management and Information System (ATMIS), Advanced Vehicle Identification (AVI), and Advanced Driver Information System (ADIS) as platforms from which IVHS can be realized. Many see these projects as a means of improving safety and efficiency of the highway system, which in turn would lead to an increase in the productivity of commuters as well as alleviate pollution[3].

Vehicle-to-vehicle communication is of critical importance to such IVHS projects, especially in Automated Vehicle Control Systems (AVCS) employing platoons [4]. Although communication occurs only over relatively short range, from less than one meter to tens of meters, the communication links have to be extremely reliable, despite the presence of multipath reflections and interference from other links using the same frequency channel.

Jakes [5] and Clarke [6] have investigated a vehicle-to-base station Rayleigh fading channel, whereas Akki and Haber [7] have investigated a vehicle-to-vehicle Rayleigh fading channel. However in this report we extend these models, to best represent a vehicle-to-vehicle channel in an IVHS setting, by considering a Rician fading channel with a direct line-of-sight component and a strong ground reflected component in a mobile-to-mobile environment.

In order to combat the effects of multipath fading and associated doppler shift as well as interference from other links multiple access schemes such as Time Division Multiple Access (TDMA), Direct Sequence Code Division Multiple Access (DS-CDMA), and Frequency Hopping with TDMA are investigated. Shladover [4] and Hitchcock [8] have shown that message delays within a platoon environment can have dire consequences. Thus the performance of these various multiple access schemes is quantified by Packet Erasure Rates (PER) as well as Reliability (probability of a successful message reception in a fixed time interval) for a given spectral allocation. Network protocol and frequency reuse in a platoon scenario will also be discussed.

This document is organized as follows. We begin in *Section 2* by discussing the platoon model in which the communication links are located and highlight various elements that will affect the channel and communication link. In *Section 3* the channel model is described. This section relies heavily upon the *Appendix*, which goes into the mathematical detail of deriving the channel model. *Sections 4 and 5* deal with the modulation and multiple access schemes that are implemented in this channel. *Section 6* discusses network protocol and frequency sharing procedures. In *Section 7* we formulate numerical results of the issues discussed in the preceding sections. *Section 8* summarizes these results and draws conclusions and recommendations of this study.

Platoon Model and Lane Capacity

2.0 Platoon Model

Shladover et. al.[4] have proposed a method of efficient vehicle control by grouping vehicles in platoons. "It requires electronically linked cars to travel in instrumented lanes with facilities to allow the vehicles to join and exit platoons smoothly at highway speeds. Estimates suggest that a [single automated lane] could carry as much traffic as three or four ordinary lanes. [Platoons of up to four cars] at speeds of *55 m.p.h.* and up have already been tested and plans to test platoons of up to *20* cars are being implemented. It is possible to obtain very accurate lane holding (within *15 cm* when under a variety of anomalous conditions) while maintaining excellent ride quality. Highway lanes could be much narrower once automated. [Thus high-precision vehicle-follower control is possible] when dynamic data obtained by ranging sensors are combined with communication between cars."[3]

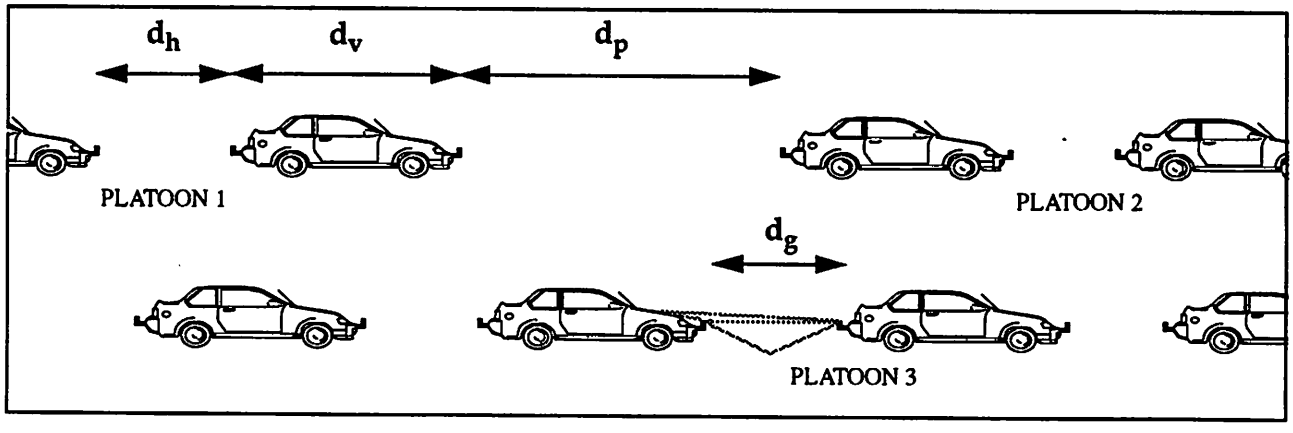

FIGURE 1. Platoon Model

We consider AVCS in a platoon environment, where a platoon consists of N vehicles. As depicted in *Figure 1*, the distance between vehicles is denoted as d_h, and is on the order of 1 or 2 meters [4]. The vehicle length, platoon following distance, and lane width are denoted as d_v, d_p, and d_l respectively, while the communication link under study is denoted as d_g.

In slotted access cellular mobile transmission schemes different cells transmit over different frequencies in order to reduce interference. Frequency bands can be reused in cells spaced far enough apart such that the interfering energy between these cells is negligible. In the platoon model each platoon (including the distance between the platoons, d_p) is considered a cell. Unlike most cellular radio schemes, the cells here are in relative motion with each other, since platoons in either lane may have a net difference in velocities. Thus we define two frequency reuse distances, d_r and d_s. The distance d_r is the reuse distance within a lane, whereas d_s is the reuse distance between lanes.

Thus for TDMA, if a cluster of C different frequencies is used, the frequency reuse distance within a lane is

$$d_r = C_r(d_p + (N-1)(d_v + d_h)) \quad \text{(EQ 1)}$$

whereas the reuse distance between lanes for both TDMA and CDMA is

$$d_s = C_s d_l. \quad \text{(EQ 2)}$$

Thus for TDMA $C=C_rC_s$ radio channels are required, each with bandwidth BT. Messages are of relatively short duration, typically a few hundreds of bits. The required transmission bandwidth is determined by the cycle duration T_c during which all vehicles in a platoon transmit their speed and acceleration data. Since CDMA transmission suppresses interference, successive platoons and platoons in other lanes may use the same bandwidths. The transmission bandwidth here is dependant on the reuse pattern between lanes and the spreading factor employed.

Radio Channel Network Model

3.0 Radio Channel Network Model

In this section we present a model for the radio channel under study. For our transmitted data to be correctly received we must ascertain the received signal power relative to any background noise in the channel and interference. As outlined in the previous section we are concerned with communication links between vehicles in a platoon. This vehicle-to-vehicle data communication will mainly consists of the continuous (routine) exchange of telemetric data such as vehicle status, speed, and acceleration. Interfering signals will be present from vehicles within the platoon and from outside the platoon (from vehicles in other lanes). Vehicles with bumper mounted directional antennas are considered.

Available propagation experiments [9], show that the vehicle-to-vehicle radio link can be modelled statistically as a Rician-fading channel. The Appendix section of this report gives an overview on Rician multipath fading and conclusions from that section are used in formulating our model. The dominant component in our Rician fading channel is likely to be relatively strong compared to the reflected signal (large Rician K-factor), and the delay spread is likely to be relatively small because reflections occur in the immediate vicinity of the transmitter and receiver antenna. We model the propagation channel as a dominant component consisting of a direct-line-of-sight wave and a ground reflected wave, a set of early reflected waves, adding coherently with the dominant wave, and intersymbol interference caused by excessively delayed waves, adding incoherently with the dominant component. The amplitude of the direct line-of-sight component will vary according to path loss, while the amplitude of the ground wave will depend on the attenuation due to reflecting of the road surface. The amplitude of the dominant path (direct line-of-sight plus ground reflected wave) will vary as the phase shift in the ground reflected wave causes interference at the receiver.

We will thus investigate two mutually independent, multiplicative propagation phenomenon: path loss and multipath fading. As shown in the Appendix multipath fading gives rise to rapid fluctuations

in the signal phase and amplitude as the vehicle travels over distances on the order of a wavelength. Whereas path loss causes variations in the signal power over tens of meters.[10] Most literature[10][5][12] also include a third propagation phenomena known as shadowing that causes power variations over distances between that of multipath fading and path loss. However since our radio link is at most 20 meters the effects of shadowing is negligible. We thus find that due to path loss the local mean signal power varies over tens of meters. Whereas due to multipath fading, within the space of a few wavelengths, our signal varies rapidly about the local mean power.

3.1 Path Loss

Propagation models proposed for micro-cellular communication, model path loss with a transition from free-space propagation to groundwave propagation if $d_g\lambda < 4h_rh_t$, where d_g is the distance of the radio link under study, h_r and h_t are the heights of the receiving and transmitting antenna respectively, and λ is the wavelength of the transmitted wave. Various models have been proposed, e.g. a step-wise transition from $\beta_1=2$ to $\beta_2=4$ (empirical values) at a certain (turnover) distance d_t. Harley[11] suggested a smooth transition, with

$$\bar{p} = d_t^{-\beta_1}\left(1+\frac{d_g}{d_t}\right)^{-\beta_2} \qquad \text{(EQ 3)}$$

again where d_t is the turnover distance. However when the distance between the receiver and antenna is small and unobstructed, as in our model, the direct line-of-sight component and the ground reflected component will cause strong fluctuations in the received signal power due to mutual interference between these two waves. Thus the local mean power of the dominant wave does not show a smooth transition between free-space and groundwave propagation. Rather this transition is marked by strong fluctuations in the local mean power.

In examining the path loss for this dominant component we must first characterize the reflection from the road surface, due to the fact that the amplitude and phase of the ground reflected wave will depend on the reflection coefficient of the road surface. The road surface is neither a perfect conductor nor dielectric so the reflection coefficient depends on the dielectric constant ε and the conductivity σ of the road surface. In order to facilitate computation we assume the road surface to be smooth and thus the dielectric constant and conductivity do not vary with distance. The reflection coefficient for horizontally polarized waves is thus given by[13]

$$\Gamma = \frac{\sin\Theta - \sqrt{\left(\frac{\varepsilon}{\varepsilon_0} - j\frac{\sigma}{\omega\varepsilon_0}\right) - (\cos\Theta)^2}}{\sin\Theta + \sqrt{\left(\frac{\varepsilon}{\varepsilon_0} - j\frac{\sigma}{\omega\varepsilon_0}\right) - (\cos\Theta)^2}}, \quad \text{(EQ 4)}$$

where ω is the angular frequency of the signal, ε_0 is the dielectric constant of free space and Θ is the angle of incidence, where we assume that angle of incidence is equal to the angle of reflection. Expressing this with ε_r the relative dielectric constant of the road surface, we obtain

$$\Gamma = \frac{\sin\Theta - \sqrt{(\varepsilon_r - j\chi) - (\cos\Theta)^2}}{\sin\Theta + \sqrt{(\varepsilon_r - j\chi) - (\cos\Theta)^2}}, \quad \text{(EQ 5)}$$

where

$$\chi = \frac{\sigma}{\omega\varepsilon_0} = \frac{18 \times 10^9 \sigma}{f}. \quad \text{(EQ 6)}$$

For vertical polarization the reflection coefficient is given by[13]

$$\Gamma = \frac{(\varepsilon_r - j\chi)\sin\Theta - \sqrt{(\varepsilon_r - j\chi) - (\cos\Theta)^2}}{(\varepsilon_r - j\chi)\sin\Theta + \sqrt{(\varepsilon_r - j\chi) - (\cos\Theta)^2}}. \quad \text{(EQ 7)}$$

Since this reflection coefficient is complex, the reflected ground wave will differ in both amplitude and phase. Yet when the angle of incidence becomes small (the distance in the radio link becomes large) the reflected wave is of equal magnitude to the incident wave with a phase shift of 180^o. However for the radio link under study the angle of incidence is usually not very small and the last approximation will not hold.

In calculating the field strength at the receiver the path difference is considered to be negligible as far as attenuation is concerned. However this path difference cannot be ignored in calculating the phase difference along the two paths. If we denote d_g as the distance of the radio link under study, h_r and h_t as the heights of the receiving and transmitting antenna respectively, and λ as the wavelength of the transmitted wave then the phase difference of the two paths is[12]

$$\Delta\varphi = \frac{2\pi}{\lambda}\left\{\sqrt{d_g^2 + (h_t + h_r)^2} - \sqrt{d_g^2 + (h_t - h_r)^2}\right\}. \quad \text{(EQ 8)}$$

If the field strength at the receiving antenna due to the direct line-of-sight wave is E_d, then the received field due to the sum of the direct line-of-sight component and ground reflected component is

$$\begin{aligned} E &= E_d[1 + |\Gamma| exp(j\angle\Gamma - j\Delta\varphi)] \\ &= E_d[1 + |\Gamma|\cos(\angle\Gamma - \Delta\varphi) + j|\Gamma|\sin(\angle\Gamma - j\Delta\varphi)] \end{aligned} \quad \text{(EQ 9)}$$

Taking the absolute value we find that

$$|E| = |E_d|[1 + |\Gamma|^2 + 2|\Gamma|\cos(\angle\Gamma - j\Delta\varphi)]^{1/2}, \quad \text{(EQ 10)}$$

and since the received power p_r is proportional to the square of the received energy we have

$$p_r = |E_d|^2[1 + |\Gamma|^2 + 2|\Gamma|\cos(\angle\Gamma - j\Delta\varphi)], \quad \text{(EQ 11)}$$

and

$$\frac{p_r}{p_t} = \left(\frac{\lambda}{4\pi d_g}\right)^2 G_t G_r[1 + |\Gamma|^2 + 2|\Gamma|\cos(\angle\Gamma - j\Delta\varphi)]. \quad \text{(EQ 12)}$$

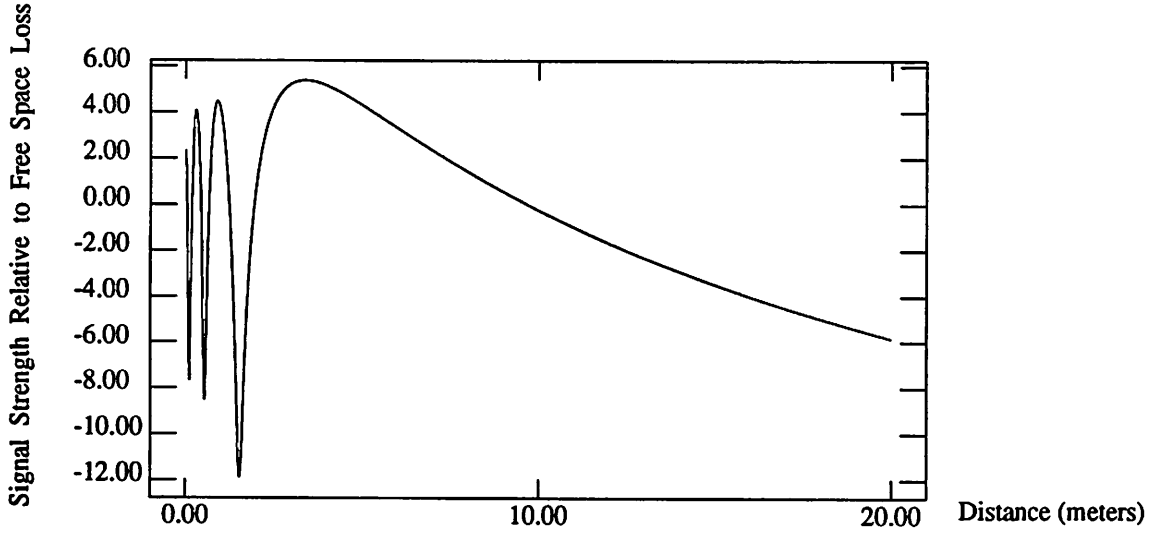

FIGURE 2. Fluctuations in Signal Power due to specular reflections of direct line-of-sight component and ground reflected wave. Here we assume $h_t = h_r = 0.5m$, $f = 1GHz$. From Parsons[12] we find the constants for the road surface to be $\varepsilon_r = 5x10^{-3}$ and $\sigma = 15$.

Thus as shown in *Figure 2*, the mean square power of the dominant component varies with distance depending on the change in phase angle of the ground wave as well as the attenuation due to the road

surface. Since this expression is intractable a closed form solution cannot be derived, we therefore calculate the local mean power given by *Eqt. 12* for every value of d_g. However from *Eqt. 12* and *Figure 2* we notice that as $d_g >> h_t, h_r$ (the angle of incidence becomes small, i.e. grazing angle) the reflection coefficient $\Gamma \rightarrow -1$. Thus *Eqt. 10* becomes

$$|E| = 2|E_d| \sin\frac{\Delta\varphi}{2}. \qquad \text{(EQ 13)}$$

Then using small angle approximation $\sin\Delta\varphi \approx \Delta\varphi$ and expressing $\Delta\varphi \approx \frac{4\pi h_t h_r}{\lambda d_g}$, both valid approximation for a large separation distance, *Eqt. 12* can be expressed as

$$\frac{p_r}{p_t} = G_t G_r \left(\frac{4\pi h_t h_r}{d^2}\right)^2. \qquad \text{(EQ 14)}$$

So for large separation distances the local mean power falls as a inverse fourth power law and is independent of frequency. On the other hand for very short distances free space loss will dominate and we see a fall off of power with an inverse square law. From this analysis and empirical values reported for path loss, we conclude that free-space loss dominates propagation between antennas of vehicles belonging to same platoon, where there is no line-of-sight component ($d_i < N\,(d_v + d_h) << d_t$) and plane earth loss for interference signals propagating from one platoon to another, where the propagation distances are large. Therefore the n^{th} vehicle in a platoon receives an normalized interference signal with power $\bar{p}_m$ from the $m+n+1^{th}$ (for $m=1,2,3...K$) vehicle given by

$$\bar{p}_m \approx m\,(d_v + d_h)^{-p_1}, \qquad \text{(EQ 15)}$$

and interference from two co-channel platoons with normalized power $\bar{p}_r$ given by

$$\bar{p}_r \approx d_r^{-(\beta_1+\beta_2)} d_t^{-\beta_2}. \qquad \text{(EQ 16)}$$

3.2 Multipath Fading

In a dispersive Rician-fading channel energy arrives at the transmitter from specular reflections as well as a dominant wave, which we define as the direct line-of-sight wave and a strong ground reflected wave. Thus the received signal of the i^{th} vehicle is in the form

$$v_i(t) = c_0 \cos(\omega_c t + \Phi_0 + \psi_i(t)) + \sum_{k=1}^{K} c_k \cos(\omega_c t + \Phi_k + \psi(t - T_k)), \qquad \text{(EQ 17)}$$

where the constant c_0 represents the amplitude of the dominant component (that is $c_0 = (1+\Gamma)d_0$ where d_0 is the amplitude of the line-of-sight component and Γ is given by *Eqt. 5*) and Φ_0 the phase delay in the dominant component. The variables c_k, Φ_k, and T_k represent the amplitudes, phases and delay times of the k^{th} reflected wave ($k = 1, 2,....,K$). Since the mobile terminal is in motion, c_k and ϕ_k are functions of time, though this is not stated explicitly. Digital phase modulation is incorporated in $\psi_i(t)$. The reflections $\{k: T_k < T_b\}$ are assumed to add coherently to the dominant component and along with the dominant component make up the first resolvable path. The remaining reflections cause intersymbol interference. During one bit time, reflections $\{k: T_k > T_b\}$ add mutually coherently and form a Rayleigh distributed phasor interfering with the first resolvable path.

We define the Rician parameter K_1 as the ratio of the power $\bar{p}_0$ in the dominant component to the local-mean scattered power $\bar{p}_1$ in the first resolvable path. The Rician parameter K_2 is defined as the ratio of the power $\bar{p}_0$ in the direct line-of-sight component to the excessively delayed local-mean scattered power $\bar{p}_2$. The local-mean power $\bar{p}$ is the sum of the power in the dominant component and the average powers in the scattered components ($\bar{p} = \bar{p}_0 + \bar{p}_1 + \bar{p}_2$). The Rician K factor, defined as the ratio of the power in the dominant component to the total scattered power is

$$K = \left(\frac{1}{K_1} + \frac{1}{K_2}\right)^{-1}. \qquad \text{(EQ 18)}$$

Since the local mean power of the dominant component varies with distance, as shown in the previous section, the above Rician parameters, although not stated explicitly, are also functions of distance.

This channel behaves as a narrowband Rician-fading channel with Rayleigh distributed intersymbol interference. For $m = 0, 1$ *or* 2 and $K_0 = 1$,

$$c_0^2 = 2\bar{p}_0 = \frac{2\bar{p}K}{1+K} \qquad \text{(EQ 19)}$$

$$\overline{p_m} = \frac{\bar{p}K}{K_m(1+K)}. \qquad \text{(EQ 20)}$$

In the following, K is assumed to be determined by the propagation environment and path length. The relative values of K_1 and K_2 are determined by the delay profile and the symbol rate. As shown in the Appendix, the instantaneous amplitude ρ of the first resolvable path has the Rician probability distribution function (pdf)

$$f_\rho\langle\rho|\bar{p}_0, \bar{p}_1\rangle = \frac{\rho}{\bar{p}_1} exp\left(-\frac{\rho^2 + c_0^2}{2\bar{p}_1}\right) I_0\left(\frac{\rho c_0}{\bar{p}_1}\right), \quad \text{(EQ 21)}$$

where $I_0(\ )$ is the modified bessel function of the first kind and zero order. Hence the probability distribution function of the signal amplitude, expressed in terms of the local-mean power $\bar{p}$ and the Rician K-factor becomes

$$f_\rho\langle\rho|\bar{p}, K\rangle = \frac{\rho(1+K)}{\bar{p}KK_1} e^{-K_1} exp\left(-\frac{\rho^2(1+K)}{2\bar{p}KK_1}\right) I_0\left(\rho K_1\sqrt{\frac{2(1+K)}{\bar{p}K}}\right), \quad \text{(EQ 22)}$$

thus for the instantaneous power we have

$$f_p\langle p|\bar{p}, K\rangle = f_\rho(\rho|\bar{p}, K)\left|\frac{d\rho}{dp}\right| = \frac{(1+K)}{2\bar{p}KK_1} e^{-K_1} exp\left(-\frac{p(1+K)}{\bar{p}KK_1}\right) I_0\left(2K_1\sqrt{\frac{p(1+K)}{\bar{p}K}}\right). \quad \text{(EQ 23)}$$

For interfering signals, the propagation distance is significantly larger, and because of the relatively low antenna height, a line-of-sight component may not be present. In such cases, Rayleigh fading appears a reasonable model.

Modulation Scheme and Bit Error Rates

4.0 Modulation Scheme

Bit Error Rates (BER) and packet erasure rates provide a relevant measure for the performance of a digital communication radio link. Most studies of average BER over fading channels only consider Additive White Gaussian Noise (AWGN) without any interference.[10] We examine the BER for the channel model proposed in the previous section (Rician fading with the dominant Rician component consisting of a direct line-of-sight component and a strongly reflected groundwave) with interference from within a platoon and co-channel interference from vehicles in other lanes. Since this model may still be too simplistic to compare performance gains from various digital modulation schemes we only consider Binary Phase Shift Keying (BPSK).

4.1 Bit Error Rates

Ideally the bit error rates for BPSK modulation in a time- invariant AWGN channels is[14]

$$P_b(e) = \frac{1}{2} erfc \sqrt{\frac{E_b}{N_0}}, \qquad \text{(EQ 24)}$$

where N_0 is the (one-sided) spectral power density of the AWGN, E_b is the constant received energy per bit $(E_b = p_0 T_b)$ and *erfc(.)* denotes the complementary error function [15]. Habbab, Kahvehrad and Sundberg [16], a later paper by Zhang and Pahlavan [17] and Linnartz, Goosen and Hekmat [18] modelled the in-phase component of Rayleigh fading co-channel interference as Gaussian noise, giving a mean error probability of

$$P_b(e|\rho, \bar{p}_r, \bar{p}_2) = \frac{1}{2} erfc \left(\sqrt{\frac{\frac{1}{2}\rho^2 T_b}{\bar{p}_r T_b + \bar{p}_2 T_b + N_0}} \right), \qquad \text{(EQ 25)}$$

where $\bar{p}_r$ is the mean co-channel interference power given by *Eqt. 16* and $\bar{p}_2$ is the mean power of the excessively delayed waves given by *Eqt. 15*. For Code Division Multiple Access (CDMA) the probability of bit error is given by

$$P_b\langle e|\rho, \bar{p}_r, \bar{p}_2\rangle = \frac{1}{2}erfc\left(\sqrt{\frac{\frac{1}{2}\rho^2 T_b}{\frac{(C_s\bar{p}_t T_b + \bar{p}_2 T_b)}{N} + N_0}}\right) \quad \text{(EQ 26)}$$

where N is the spreading factor of the CDMA scheme and C_s is the frequency reuse factor between lanes. The average BER can then be found by integrating over the Rician pdf of the signal amplitude given in *Eqt. 22*

$$\bar{p}_b = \int_0^\infty \frac{\rho(1+K)}{\bar{p}KK_1} e^{-K_1} exp\left(-\frac{\rho^2(1+K)}{2\bar{p}KK_1}\right) I_0\left(\rho K_1\sqrt{\frac{2(1+K)}{\bar{p}K}}\right) \times P_b\langle e|\rho, p_r, p_2\rangle d\rho \,. \quad \text{(EQ 27)}$$

Since amplitude of the signal varies with distance (and as time as well since velocity is distance per time) the bit error rate will vary with distance (and time).

Multiple Access Schemes and Packet Erasure Rates

5.0 Multiple Access Schemes

In our platoon model many vehicles will be vying for access to our transmission medium. In order to guarantee reliable communication we must consider multiple access schemes which will allow vehicles access to the transmission medium without excess delays. We compare a slotted Time Division Multiple Access (TDMA) with a Code Division Multiple Access Scheme (CDMA). Because of the short communication range and the corresponding small delay spread, CDMA to avoid narrowband fading of the signal may require prohibitively large spreading factors. Therefore we use spreading mainly to suppress interference. Also the problem of dynamic power control for multiple receiver positions may affect the efficiency of spread spectrum for AVCS environment. Since the channel is likely to be constant only for periods during which the vehicle moves less than $\lambda/6$ meters, efficient and reliable link design requires messages from each vehicle to be shorter than a few milliseconds. This would be easier to achieve in high speed unspread burst (TDMA) transmission, since for a system with fixed bandwidth any spreading by a factor N implies an increase in transmission time by a factor N. On the other hand with CDMA continuous wave (CW) transmission is possible, which allows simpler synchronization and avoids large overheads for power on/off synchronization times. In this section we compare TDMA, TDMA with slow frequency hopping interferers, and Direct Sequence CDMA (DS-CDMA) with regards to Packet Erasure Rates (PER). In the next section we analyze these same multiples access schemes with regard to reliability and spectrum allocation.

5.1 Packet Erasure Rates

A packet erasure can occur when bit errors are in excess of the correcting capabilities of the error correction coding being implemented. In this section we describe some of the analytical models that may be used to evaluate the probability of packet erasure. *Slow* and *fast* Rician fading of the wanted signal are considered with a block error detection code that can correct up to M errors in a block of L bits.

5.1.1 Code Division Multiple Access

With fast fading, the duration of the packets is substantially longer than the time constants of the multipath fading. This is the case with continuous wave CDMA transmission with a bit rate of *5 kbits/sec* and a carrier frequency of *1 GHz* and vehicle speed of *30m/s (~70 miles/hour).* In this case the received signal experiences several fades during packet transmission. For DS-CDMA packet erasure rates are found assuming fast fading. DS-CDMA accomplishes multiple access by multiplying every bit with a faster chip sequence *c(t).* The transmitted signal *s(t)* for DS-CDMA is

$$s(t) = a(t)\,c(t)\cos\omega_c t \qquad \text{(EQ 28)}$$

We assume that during one bit time, the channel characteristics do not change. Then during reception of a packet, each signal is expected to experience several fades. It is also assumed that the received amplitude and phase of all signals are statistically independent from bit to bit even though the receiver remains perfectly locked to the wanted signal. Then the probability of correctly receiving a packet is same as receiving M independent bits out of L bits, which is a binomial distribution. So the probability of undetected packet errors for BPSK is obtained from

$$P\langle e|\bar{p}_o, \bar{p}_r\rangle = 1 - \sum_{m=0}^{M} \binom{L}{m} (1-\bar{p}_b)^{L-m} (\bar{p}_b)^m \qquad \text{(EQ 29)}$$

where the average bit error probability $\bar{p}_b$ is defined in *Eqt. 27.*

5.1.2 Time Division Multiple Access

Slow fading occurs when packets are of sufficiently short duration, that the received amplitude and carrier phase may be assumed to be constant throughout the duration of the packet. This condition is satisfied if the motion of the mobile terminal during the transmission time of a block of bits is negligible compare to the wavelength. This is the case with burst transmission TDMA at a bit rate of *5kbits/sec* with an average frame of *20 cars/platoon.* If we have make the approximation that the interfering sample is Gaussian distributed with mean $\bar{p}_r$, and that interference samples between successive bits are statistically independent, then the probability of packet erasure in a block of *L* bits with *M* bit correction is found by averaging the probability of packet error over the Rician fading of the wanted signal, that is

$$P\langle e|\bar{p}_o, \bar{p}_i\rangle = \int_0^{\infty} \frac{(1+K)}{2\bar{p}KK_1} e^{-K_1} exp\left(-\frac{p(1+K)}{\bar{p}KK_1}\right) I_0\left(2K_1\sqrt{\frac{p(1+K)}{\bar{p}K}}\right)$$

$$\times \left\{1 - \sum_{m=0}^{M} \binom{L}{m} \left(1 - \frac{1}{2} erfc\left(\sqrt{\frac{pT_b}{\bar{p}_r T_b + \bar{p}_2 T_b + N_0}}\right)\right)^{L-m} \left(\frac{1}{2} erfc\left(\sqrt{\frac{pT_b}{\bar{p}_r T_b + \bar{p}_2 T_b + N_0}}\right)\right)^{m}\right\} dp \ . \quad \text{(EQ 30)}$$

Co-channel interference may be much greater in TDMA schemes than CDMA schemes. Since in CDMA these interference signals are spread or made to resemble noise, whereas in TDMA these co-channel interference signals are not processed at all. Slow frequency hopping can be employed to reduce this effect. With this scheme a different carrier frequency is chosen at the end of every packet reception according to a pseudo-random hopping sequence. Thus the effects of co-channel interference is diminished. This increase in performance is achieved at the cost of increase in bandwidth.

Network Protocol

6.0 Network Protocol

In a TDMA scheme there must be some protocol within a platoon in order for information to pass from one vehicle to the next efficiently. We ignore frame synchronization checking and define the radio protocols as follows: the lead vehicle transmits its report, upon reception of a report by the n^{th} vehicle, the $n + 1^{th}$ vehicle send its report. The performance or the radio link can be quantified by the probability that a message can be successfully transmitted across a platoon from one vehicle to another. We define the completion of a message through a platoon in this manner as a cycle. If a vehicle does not recognize a message or erroneously detects a message a cycle is interrupted. To ensure safe operation of the AVCS vehicle control system, we require a very small probability of undetected errors. On the other hand we wish a large probability that a cycle is completed successfully. The n^{th} vehicle transmits its report after it has successively received messages with bit pattern which differed in less than M_2 places from a valid codeword of the $n\text{-}1^{th}$ vehicle. A message is assumed to be received successfully and reliably if the detected bit sequences does not differ in more than M_1 places from a valid code word. It is not necessary to take $M_1 = M_2$. In fact if $M_1 < M_2$, the terminal may transmit its own status assuming that it's turn to transmit has arrived, yet not entirely relying upon the data in the received packet because of a large number of bit errors. The performance of the network is quantified by finding the probability that the $n\text{-}1^{th}$ vehicle successfully transmits its report to the n^{th} vehicle, with $M_1 < M_2$. In an AVCS environment the lead vehicle generates data that all vehicles in the platoon require[4], thus we are also interested in the probability that the lead vehicle successfully transmits its report to the n^{th} vehicle, with $M_1 = M_2$.

6.1 Reliability and Spectrum Allocation

Finite transmission speed and message delays cause packet losses on the radio channel, Hitchcock[8] has shown that these delays can have dire consequences in the performance of the system. In order to

study the reliability of the system, a "reliability" measure R is defined as the probability that at least one successful update occurs during a period T. This does not imply that the entire AVCS system has a certain reliability R, and will result in a vehicle collision on an average of $T/(1-R)$ seconds. Given a reliability measure (R,T) we assume that the safety and control measures of the system perform within given parameters[8]. For a given reliability, the spectrum occupation is dependant on the multiple access scheme and frequency reuse pattern implemented. Thus spectrum allocation for a required reliability can be used in comparing the various multiple access schemes of the previous section.

Numerical Results

7.0 Numerical Results

The previous sections detailed the modelling of the communication channel under study and derived various parameters that quantify the performance of this communication link. In this section we present numerical results of these parameters. In formulating these results certain assumptions were made for all simulations. As described in *Section 2* and depicted in *Figure 1*, the average length: of a vehicle, d_v, was assumed to be *5 meters*, of the lane width, d_l, was assumed to be *3 meters*, of the distance between automated cars, d_h, was assumed to be *1 meter*, and the average velocity of an automated vehicle was assumed to be *70 m.p.h.* The distance of the radio link under study, d_g, was varied from *0.1 meters* to *10 meters*. As explained in the *Appendix*, a carrier frequency of *1 GHz* was assumed and a bit rate of *5 kbits/sec*. From Bultitude and Bedal[34], we know that $K = 7dB$ $(K_1 \approx 5)$ is reasonable for most micro-cellular channel, we assume $K_1 = 10$ as an upper bound. Since all vehicles transmit data with the same power, the signal to noise (AWGN Gaussian) ratio was set to *10dB* at $d_g = 10$ *meter* and *30dB* at $d_g = 1$ *meters*.

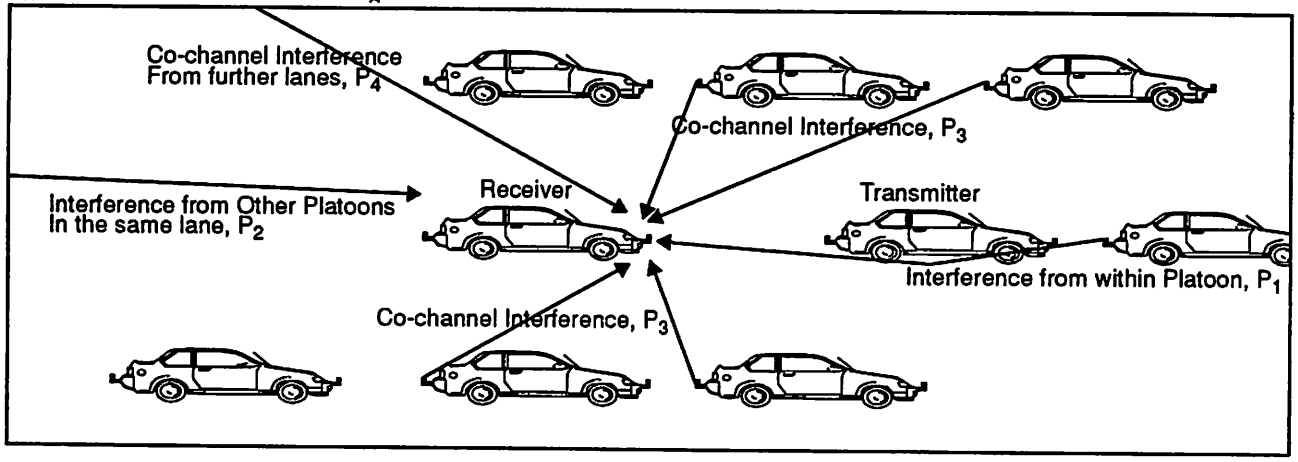

FIGURE 3. Assumptions about Interference in radio link

As explained in *Section 3* and shown in *Figure 3*, the radio link suffers from interference from within its' platoon (P_1), from platoons in the same lane (P_2), and co-channel interference from platoons in other lanes (P_3 and P_4). In all simulations we assume that the target vehicle is joining an infinitely long platoon. Thus, d_g varies and the we get a upper bound on P_1. It should be noted that in TDMA transmission each vehicle within a platoon is given a time slot in which to transmit, thus P_1 will be zero; while for CDMA type transmission all vehicles transmit at the same time, thus P_1 must be taken into account. We assume P_2 is negligible since transmissions from other platoons must be reflected off vehicles, road surface, and surroundings before reaching the receiver. These reflections will greatly attenuate the signal. We thus set $d_r = C_r = 0$ from *Eqt. 2*. To obtain an upper bound on the P_3 and P_4 we assume that an infinitely long platoon would transmit as close as possible to the receiving vehicle. Lacking accurate measurements, it was assumed that these signals would attenuate by *10 dB* for each lane traversed, thus P_4 would be *10 dB* less than P_3.

7.1 Bit error rates

We will first show bit error rates (BER) as a function of distance as described in *Eqt. 25*, *Eqt. 26*, and *Eqt. 27* and compare them to a channel model in which a strongly reflected ground wave is not present.

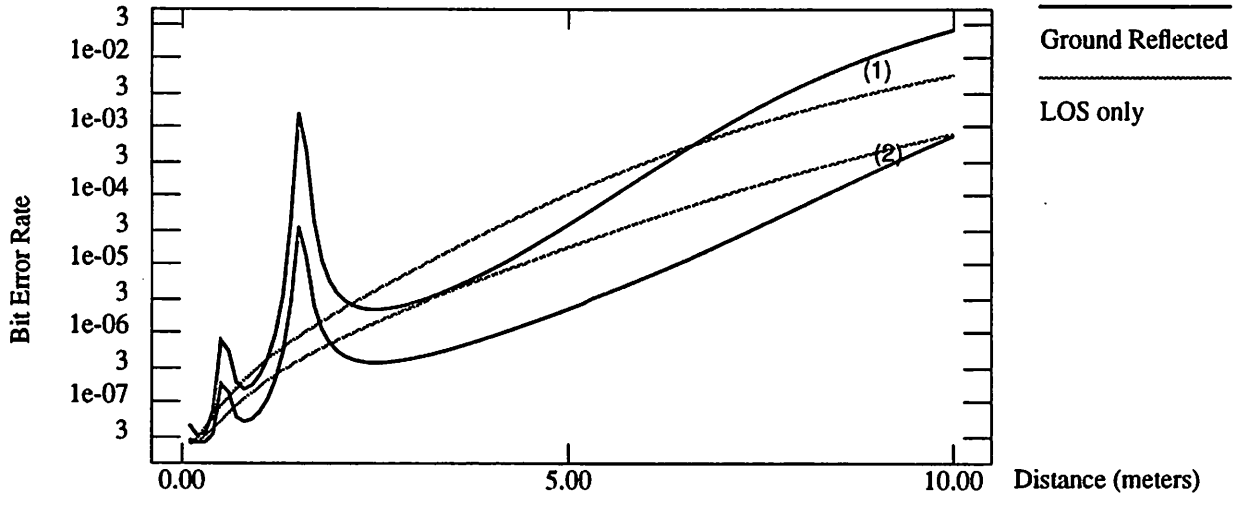

FIGURE 4. Comparison of Ground Reflected Wave (horizontal polarization) plus Direct Line-of-sight (LOS) Channel Model with only LOS model for CDMA bit error rates. (1) C_r=1 N=32 (2) C_r=3 N=32.

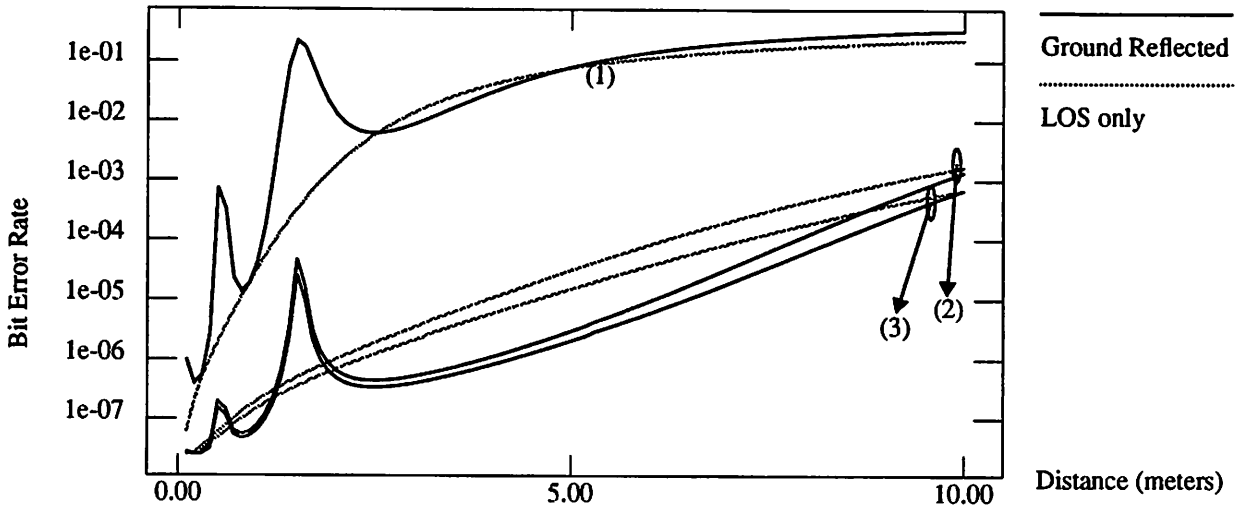

FIGURE 5. Comparison of Ground Reflected wave plus Direct Line-of-sight (LOS) Channel Model (where all waves are horizontally polarized) with only LOS model for TDMA bit error rates. (1) C_r=1 (2) C_r=3 (3) C_r=6

Figures 4 and 5 compare the channel model described in *Section 3* (with horizontal polarization) with a channel model that neglects a strongly reflected ground wave. We see that both models converge to a BER of 0.5, which is intuitive since as the link distance is increased we are left with noise and have approximately 50% chance of deducing the correct bit if both input bits are equiprobable. It is interesting to note that smaller values of reuse patterns result in a quicker convergence between the two models, since fewer reuse frequencies result in more interference and thus faster degradation of the communication link. Also the ground wave model shows great variations in BER for distances less than three meters. This is as expected since for distances less than three meters the ground wave and line-of-sight component interfere and cause deep fades in the wanted signal.

Figure 6 examines the effect of varying the reuse pattern C_r and the spreading factor N for CDMA transmission employing horizontal polarization. From this figure it is evident that for both $N=32$ and $N=128$ the bit error rates show a great change only when $C_r=1$. When the reuse pattern is greater than one the bit error rates remain relatively the same independent of spreading factor and reuse pattern. Thus we will concentrate on CDMA with a reuse factor $C_r=2$ and a spreading facto $N=32$, since this will give nearly the same performance as other schemes, but with minimal bandwidth.

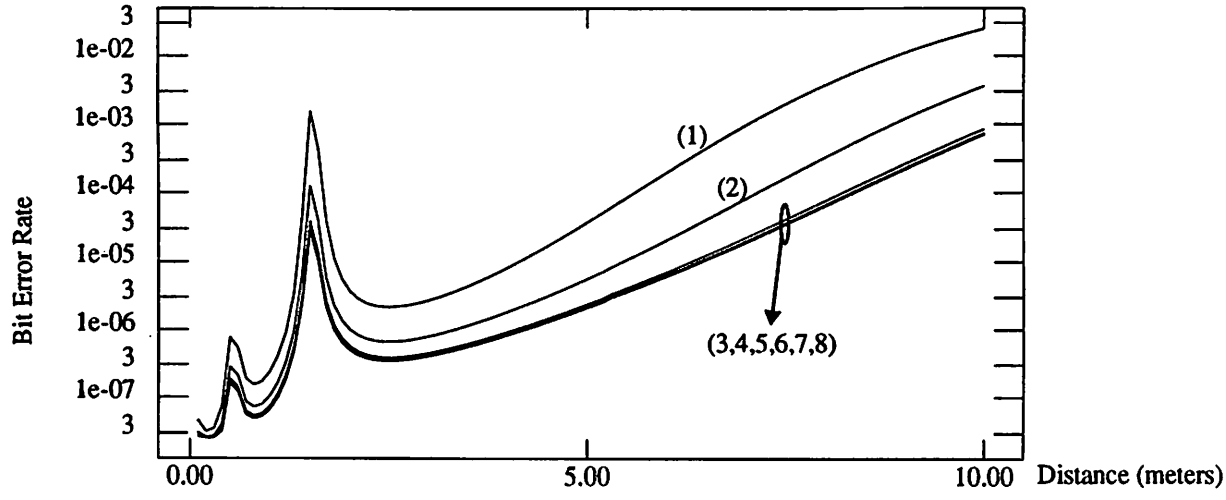

FIGURE 6. Bit error rates for CDMA with horizontal polarization and various spreading factors (N) and frequency reuse factors (C_f). (1) C_f=1 N=32 (2) C_f=1 N=128 (3) C_f=2 N=32 (4) C_f=3 N=32 (5) C_f=6 N=32 (6) C_f=2 N=128 (7) C_f=3 N=128 (8) C_f=6 N=128.

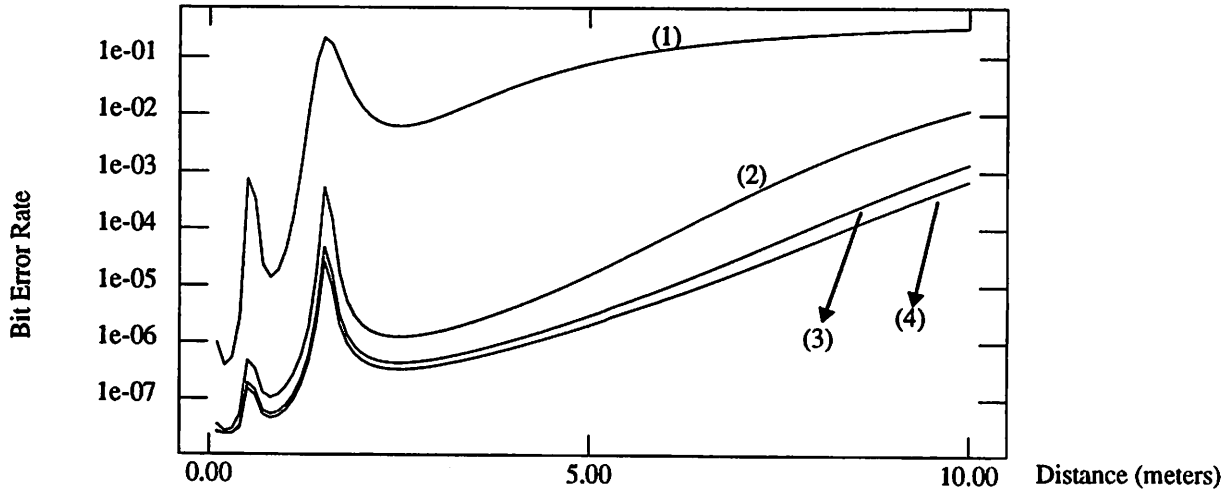

FIGURE 7. Bit error rates for TDMA with horizontal polarization and various frequency reuse factors (C_f). (1) C_f=1 (2) C_f=2 (3) C_f=3 (4) C_f=6.

The effects of varying frequency reuse patterns for TDMA is presented in *Figure 7*. Here we see that unlike the CDMA case varying the reuse pattern has a significant impact on the bit error rates, thus TDMA is more sensitive to interference than CDMA. However as C_r increases the gain in performance decreases. So by using more bandwidth (increasing C_r) we get smaller and smaller gain in performance (lower BER). We will concentrate on TDMA with a reuse pattern of $C_r=3$.

Both vertical and horizontal polarization is considered in the next two figures. With vertical polarization bit error rates do not deteriorate as badly as horizontal polarization for distances less than 3 meters. For distances greater then three meters the bit error rates for vertical polarization are greater than horizontal polarization. However as the reuse factor increases this variations diminishes, while the larger variations within three meters are still present.

Figure 10 compares bit error rates of our system employing CDMA and TDMA. It should be noted that these two systems require different bandwidths. This curve again emphasizes the need of some frequency reuse, since bit error rates with $C_r=1$ give poor performance. It should also be noted that for CDMA with $C_r=2$ $N=32$ (5) and TDMA with $C_r=3$ (4) the bit error rate performance is nearly the same.

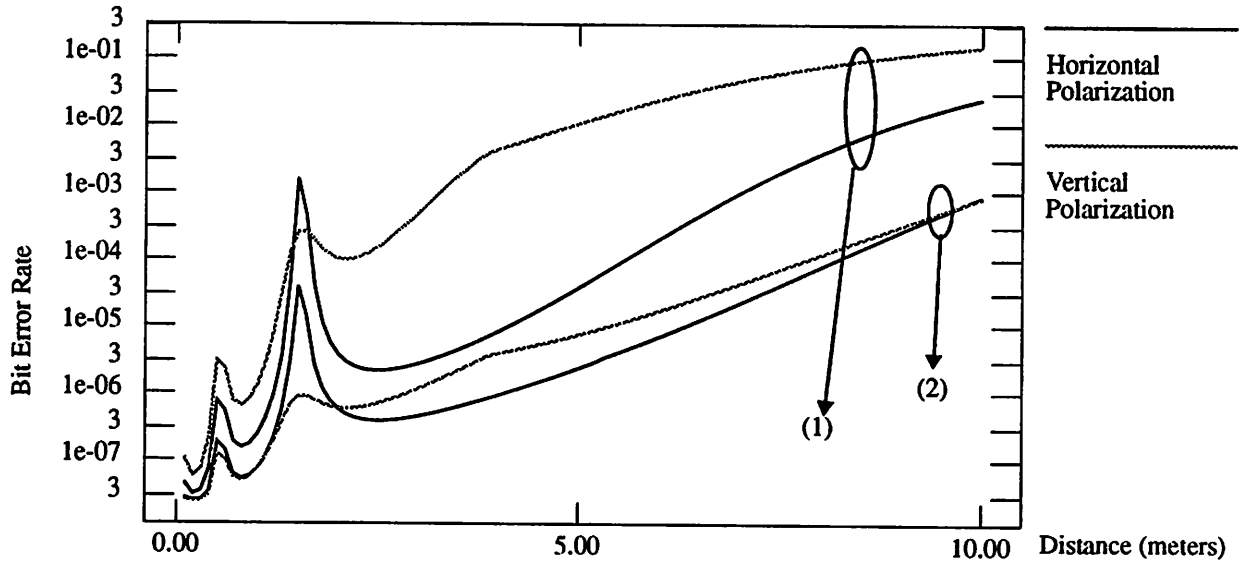

FIGURE 8. Bit error rates for CDMA N=32 with vertical and horizontal polarization. (1) C_r=1 (2) C_r=2.

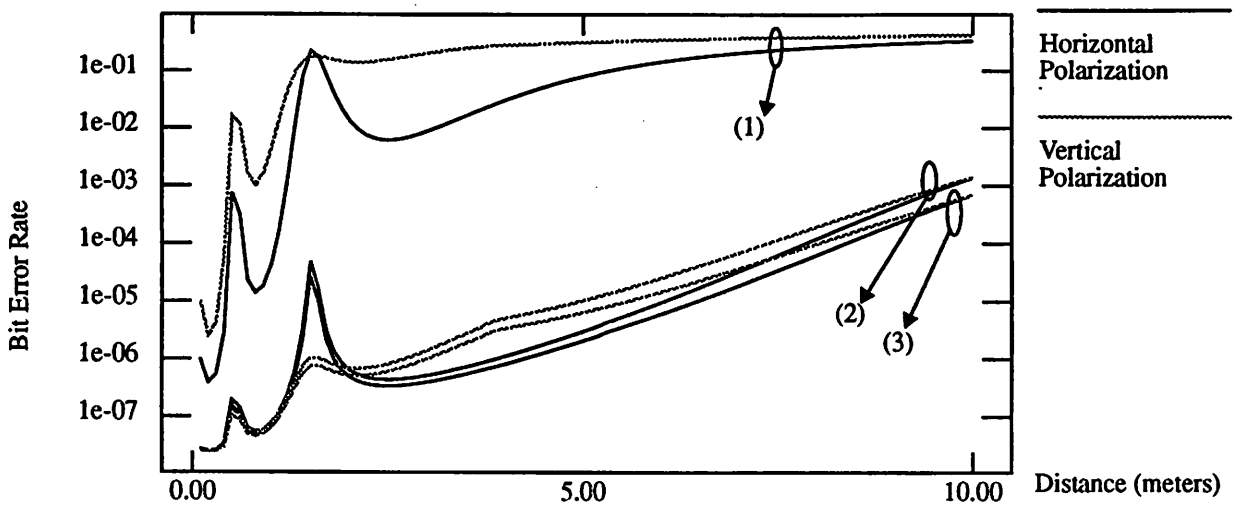

FIGURE 9. Bit error rates for TDMA with vertical and horizontal polarization. (1) C_f=1 (2) C_f=2. (3) C_f=6.

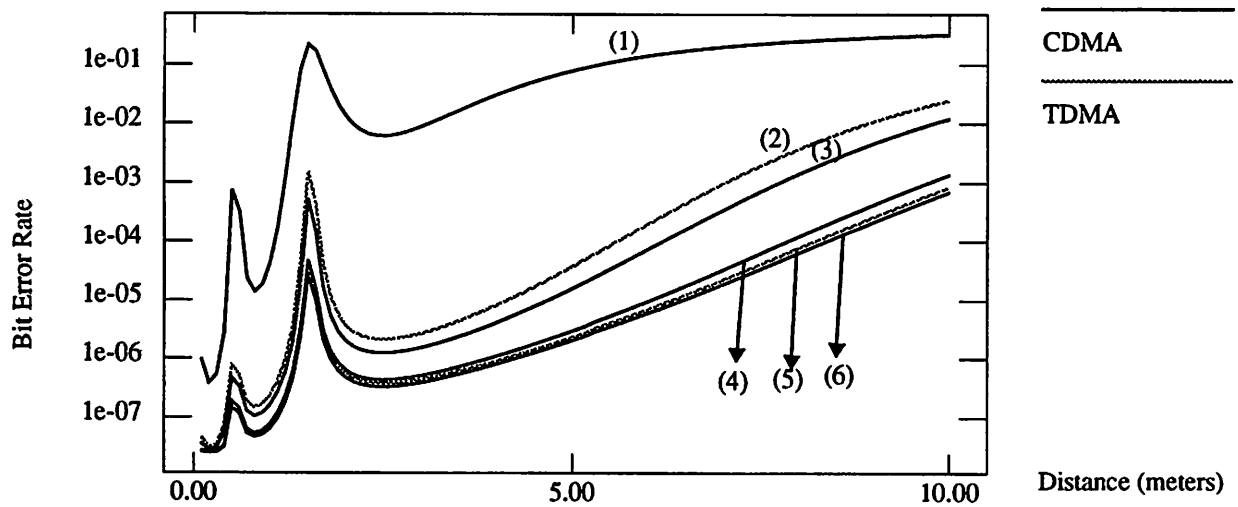

FIGURE 10. Comparison of bit error rates for TDMA and CDMA employing horizontal polarization. (1) C_f=1 (2) C_f=1 N=32 (3) C_f=2 (4) C_f=3 (5) C_f=2 N=32 (6) C_f=6.

7.2 Packet Erasure Rates

Numerical results of packet erasure rates as described in *Section 5* are presented in this section. As explained in *Section 5* we assume a fast fading channel for CDMA and a slow fading channel for TDMA, which results in *Eqt. 29* and *Eqt. 30*. We also assume the same interference as in stated in *Section 7.0* and a packet length (*L*) of *76 bits* with (*M*) one bit correction[36]. We first show that many of the bit error rate results of *Section 7.1* are not affected by fading and thus can be applied to packet erasure rates.

Figures 11 depicts packet erasure rates (PER) for CDMA with various spreading factors. As with BER results, a reuse factor other than one results in curves that are relatively the same regardless of spreading factor. Thus we will concentrate on CDMA with $C_r=2$ and $N=32$. *Figure 12* depicts PER curves for TDMA with various reuse factors. Again as with BER curves, the reuse factor does play an important role. As the reuse factor is increased the PER tends to converge. Thus we will concentrate on TDMA with a reuse factor of $C_r=3$.

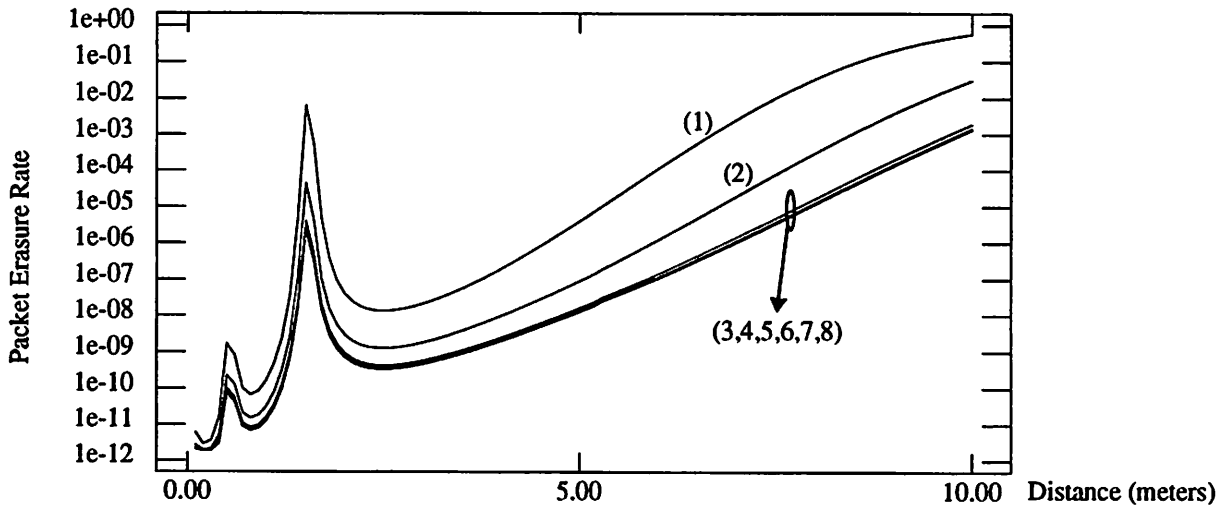

FIGURE 11. Packet erasure rates for CDMA with horizontal polarization and various spreading factors (N) and frequency reuse factors (C_r). (1) C_r=1 N=32 (2) C_r=1 N=128 (3) C_r=2 N=32 (4) C_r=3 N=32 (5) C_r=6 N=32 (6) C_r=2 N=128 (7) C_r=3 N=128 (8) C_r=6 N=128.

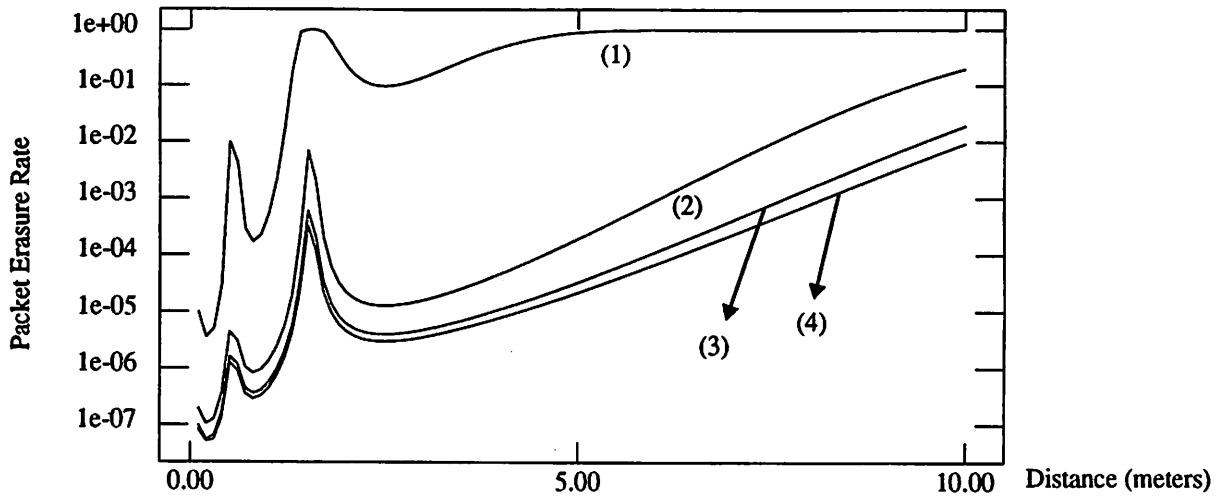

FIGURE 12. Packet erasure rates for TDMA with horizontal polarization and various frequency reuse factors (C_f). (1) C_f=1 (2) C_f=2 (3) C_f=3 (4) C_f=6.

Figure 13 compares TDMA and CDMA packet erasure rates with horizontal polarization, again it should be noted that these system require different bandwidths. Although in *Figure 10*, the bit error rates for TDMA with $C_r=3$ and CDMA with $C_r=2$ $N=32$ were nearly identical, the packet error rates for the same situation differs significantly due to the nature of fading in each scheme. In order to increase the performance of TDMA we introduced the concept of Slow Frequency Hopping in *Section 5*. By this we mean that within each platoon a TDMA type polling scheme is implemented. However a different carrier frequency for each platoon is chosen, according to a pseudo-random hopping sequence, at the end of every packet reception. Thus from *Figure 3*, the co-channel interference power P_3 and P_4 are reduced since there is a greater probability that adjacent lanes use different carrier frequencies. It should be noted that for a reuse pattern $C_r=2$, two independent sets of hopping frequencies (H) are required.

Figure 14 illustrates slow frequency hopping as outlined above with various reuse factors and two sets of hopping frequencies. It is evident that a reuse factor of $C_r=3$ and a set of $H=10$ hopping frequencies will give optimum performance.

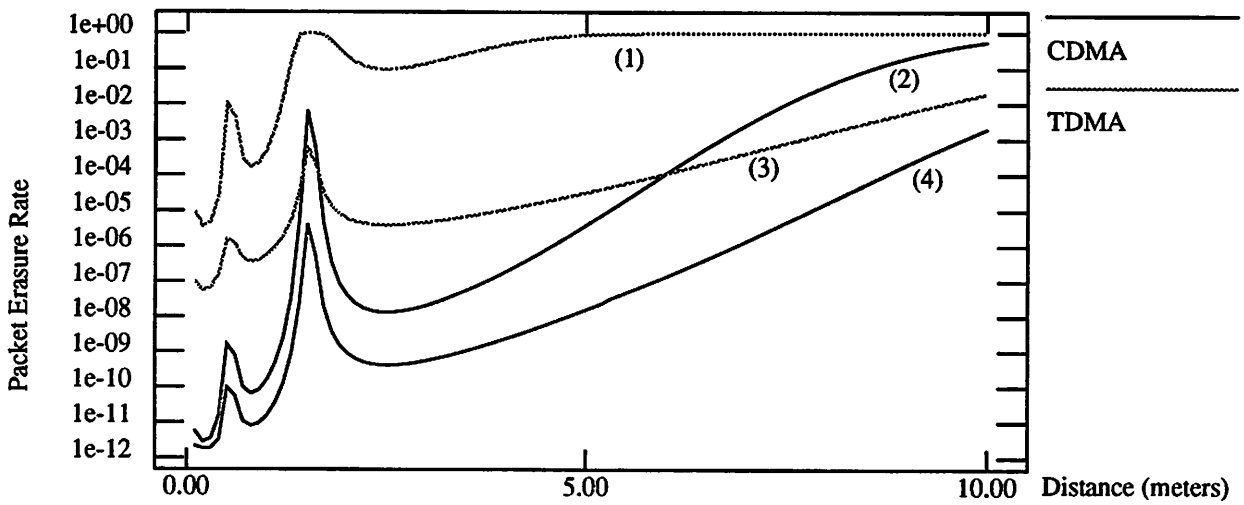

FIGURE 13. Comparison of packet erasure rates for TDMA and CDMA schemes employing horizontal polarization. (1) C_r=1 (2) C_r=1N=32 (3) C_r=2 (4) C_r=3 (5) C_r=2 N=32 (6) C_r=6.

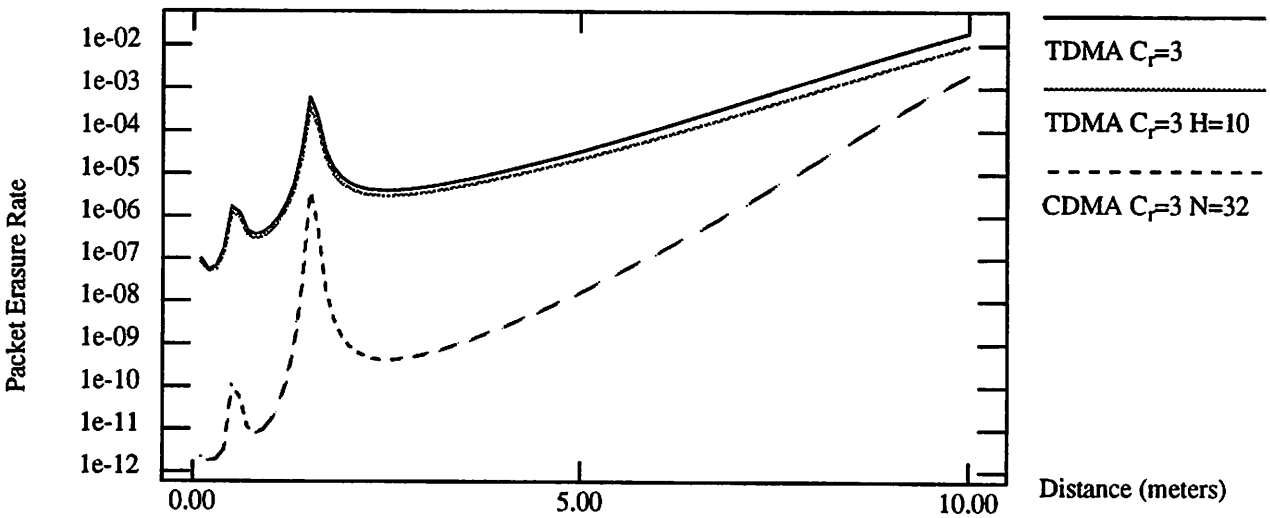

FIGURE 15. Comparison of CDMA, TDMA, and slow frequency hopping.

Comparing TDMA $C_r=3$, TDMA $C_r=3$ and $H=10$, and CDMA $C_r=2$ $N=32$ in *Figure 15* we see that

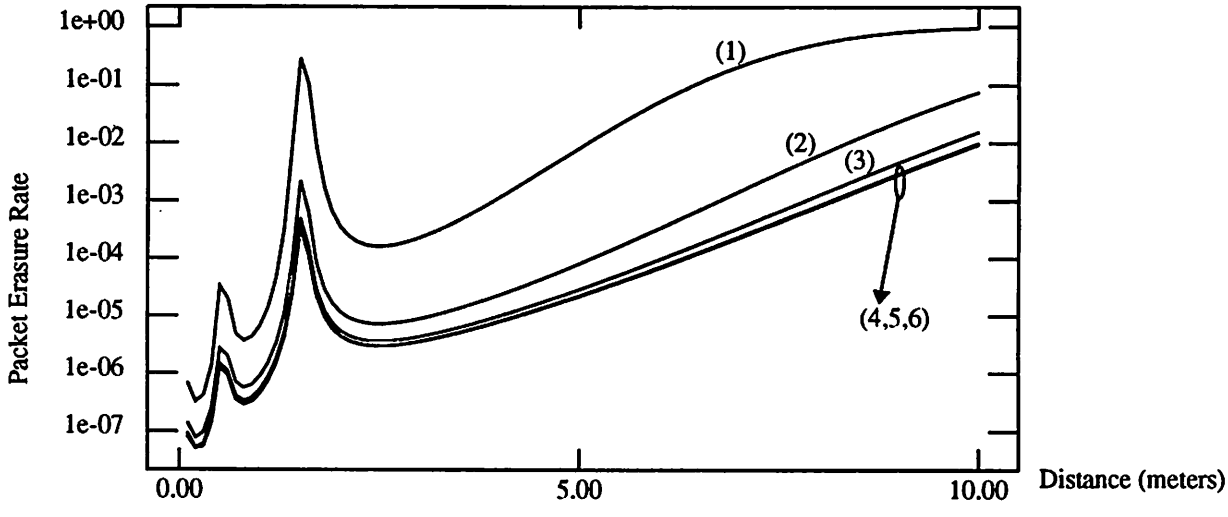

FIGURE 14. TDMA with slow frequency hopping for various reuse factors (C_r) and Hopping Frequencies (H). (1) C_r=1 H=10 (2) C_r=1 H=100 (3) C_r=2 H=10 (4) C_r=2 H=100 (5) C_r=3 H=10 (6) C_r=3 H=100.

the slow frequency hopping scheme does better than TDMA but CDMA still out performs both schemes. It still must be noted that all three schemes require different bandwidths.

Lastly we see in *Figure 16* that packet erasure rates, for both CDMA and TDMA, with vertical polarization yields better results for distances less than three meters and slightly higher packet erasure rates for distances greater than three meters.

7.3 Reliability and Spectrum Allocation

In the previous section it was stated that the systems we compared did not have the same bandwidth requirements. In this section we quantify the different bandwidth requirements of the previous schemes by presenting numerical analysis results of Reliability vs. Spectrum Allocation as described in *Section 6.1*. Reliability $R(T,d_g)$ is defined as the probability a message does not pass through a our communication link in time T when the vehicles are at a distance d_g. Other sources also refer to this as the deadline failure probability in other sources. In our results we have assumed a maximum delay time $T=50\ msec$ at a link distance $d_g=10m$[4].

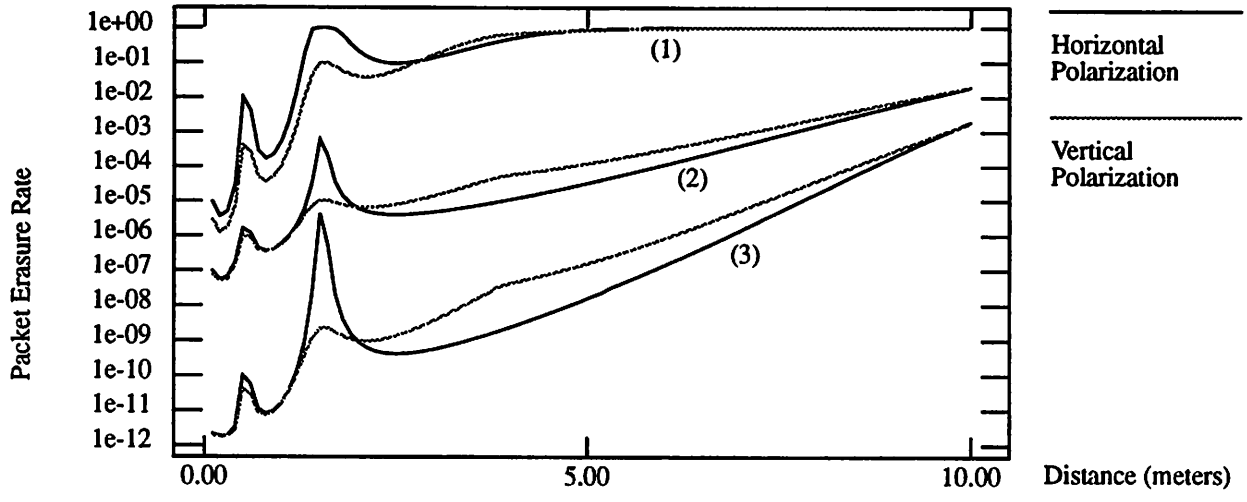

FIGURE 16. Comparison of TDMA and CDMA packet erasre rates for horizontal and vertical polarization. (1) TDMA C_r=1 (2) TDMA C_r=3 (3) CDMA C_r=2 N=32.

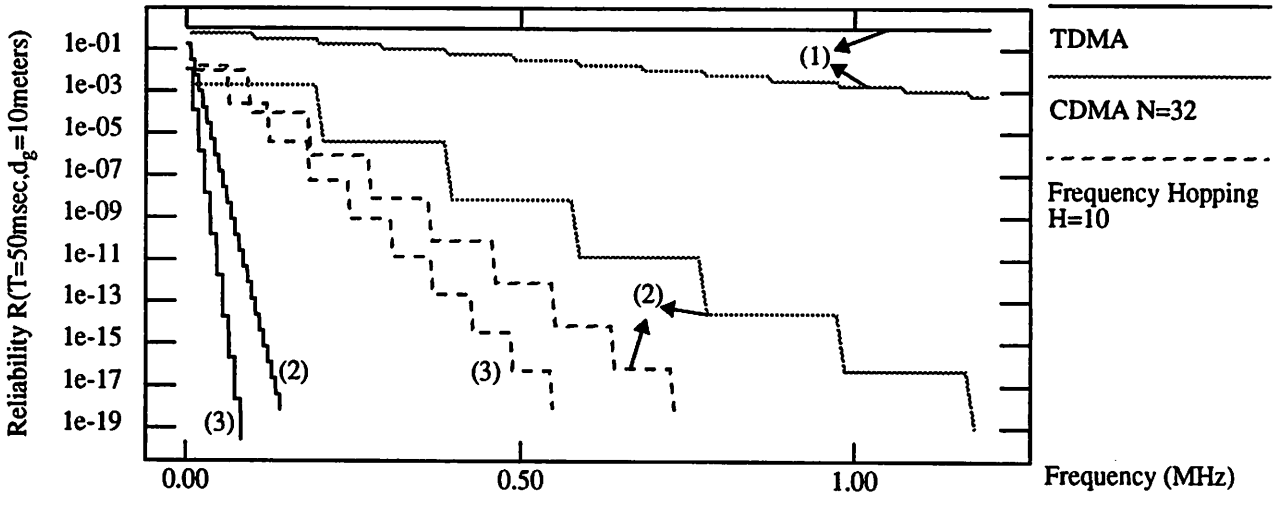

FIGURE 17. Reliability vs. Spectrum allocation for CDMA, TDMA, frequency hopping. (1) C_r=1 (2) C_r=2 (3) C_r=3.

Figure 17 illustrates that although CDMA C_r=2 N=32 gave much better PER results than TDMA, it

requires much more bandwidth. Thus we can implement TDMA by requiring many retransmissions and although many of these transmissions would be lost, we are guaranteed a successful transmission using less bandwidth than CDMA. The gain in PER by frequency hopping also came as a result of greater bandwidth requirements, although not as much as CDMA. Again it is evident that $C_r=1$ does not yield desirable results, simply because at $d_g=10m$ the PER is so high that many retransmission are required. Interestingly TDMA $C_r=3$ requires less bandwidth for a given reliability than TDMA $C_r=2$, since even though TDMA $C_r=3$ requires more frequency bands per lane, the gain in PER is great enough that fewer retransmissions are required. We see that for frequency hopping this in not true.

7.4 Network Protocol

Section 6.0 described a network protocol for TDMA transmissions. The concept of a complete cycle through a platoon was developed and the idea propounded that a cycle could be maintained without retransmission even though the received codeword differed from a valid code word by more than the error correcting capabilities of the code being used. Again employing the assumptions of the previous sections, it is shown how variations in M_1 (correcting capabilities of the code) and M_2 (errors in received codeword) affect the probability of cycle completion for both TDMA and frequency hopping.

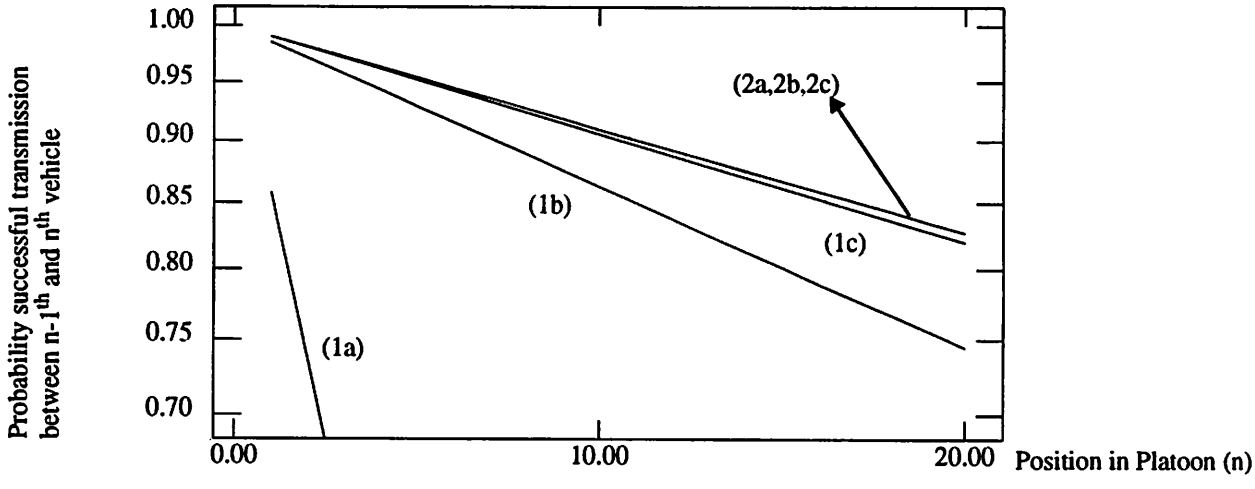

FIGURE 19. Probability lead vehicle transmits to n^{th} vehicle vs. n, $M_1=M_2=1$, L=76, d_h=10m. (1) C=3 (2) C=6 (a) H=1 (b) H=10 (c) H=100

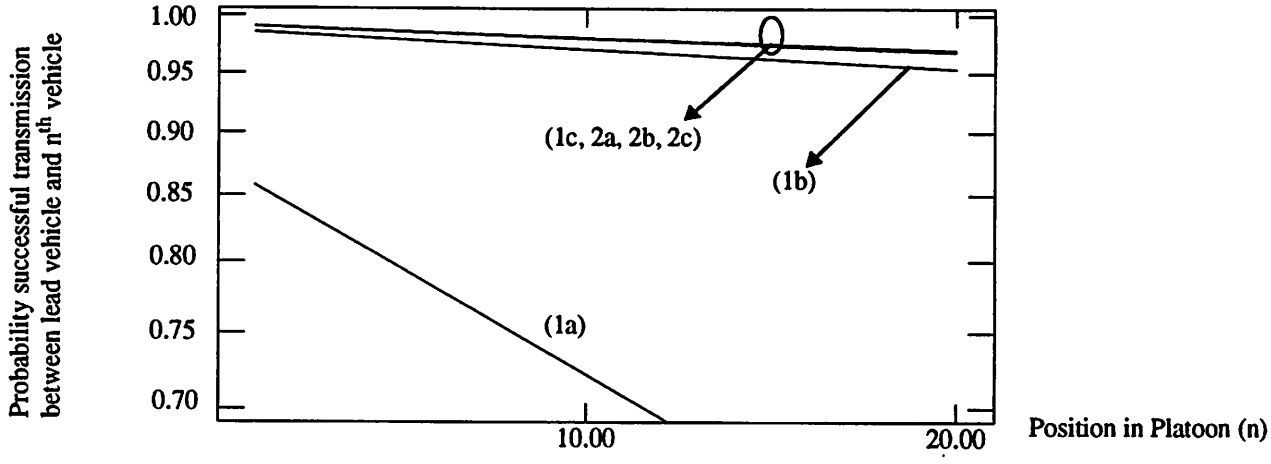

FIGURE 18. Probability n-1th vehicle transmits to nth vehicle vs. n, M_1=1, M_2=5, L=76, d_h=10m. (1) C=3 (2) C=6 (a) H=1 (b) H=10 (c) H=100.

Figures 18 and 19 illustrate how varying M_1 and M_2 will affect the network. The probability of successful transmission between two links in *Figure 18*, requires all links to have less than M_1 errors. While in *Figure 19* only the link between *n-1*th and n^{th} vehicle need to have less than M_1 errors, while the *n-2* prior links need only to have less than M_2 errors. Thus for TDMA it is critical that a cycle be maintained. While for CDMA all vehicles transmit simultaneously, thus preservation of the cycle is not as important.

Conclusions

8.0 Conclusions

In this report a statistical model of a vehicle-to-vehicle radio channel, with regards to AVCS communication, was developed taking into account multipath reflections and a dominant wave composed of a direct line-of-sight wave with a strongly ground reflected wave. The performance of this radio link was gauged by bit error rates, packet erasure rates, and reliability for a given bandwidth. These parameters were analytically and numerically evaluated for three multiple access techniques: Time Division Multiple Access, (Direct Sequence) Code Division Multiplexing Access, and Time Division Multiple Access within a platoon with Frequency Hopping outside the platoon.

It was evident from our analysis that our channel was highly vulnerable to deep fades (and thus large probability of packet loss) for distances less than three meters due to the interference of the ground reflected wave and the direct line-of-sight wave. The effects of these fades could be reduced by employing vertical polarization as opposed to horizontal polarization. However for distance greater than three meters, horizontal polarization PER and BER performance showed an improvement over vertical polarization. The performance difference between polarization techniques for distances greater than three meters could be mitigated by decreasing co-channel interference (increasing the frequency reuse pattern thus increasing bandwidth). Thus if frequency reuse between lanes is employed, vertical polarization can be implemented in order to mitigate the effects of deep fades caused by the interference between the ground reflected wave and the direct line-of-sight wave.

The channel under study was also found to be sensitive to co-channel interference. Our analysis showed that even for CDMA transmission performance could be largely improved if adjacent lanes use different frequencies. However, increasing the reuse factor greater than two, for CDMA, and three, for TDMA, did not afford better performance. According to our computations and within the validity of our assumptions, CDMA provides lower packet erasure probabilities than TDMA or slow frequency hopping. However for a fixed bandwidth system, the reliability for a given bandwidth or

delay line failure probability appears to be better with TDMA. Here we see a trade off between error probabilities and bandwidth. With CDMA increasing bandwidth results in lower error rates. However with TDMA even though the error rates may be greater than CDMA, many retransmissions are possible since the bandwidth requirements of TDMA are minimal compared to CDMA. TDMA also affords the system designer to implement a protocol scheme in which correct packet reception is not necessary in order to transmit an update to the next vehicle. As our analysis showed by varying the allowable number of bit errors in a received packet the delay in a TDMA system can further be reduced. All these factors should be taken into consideration in developing a communication system within such a channel.

Appendix: Channel Characterization

A1.0 Introduction

The application of microwave data links in a land-to-mobile environment has been shown to suffer from multipath fading, shadowing, and Doppler phase shifts. These effects limit the performance of the system. It is thus desirable to have a model of the channel and its limiting effects. In this section a statistical model is developed for a narrowband mobile-to-mobile channel taking into consideration Rician scattering near receiving and transmitting antennas both individually and concomitantly. From the proposed channel model we obtain, the probability density function of the received signal envelope, the time correlation function and RF spectrum of the received signal, and level crossing rates and average fade durations. We discuss the impact of these parameters on communication networks supporting an Intelligent Vehicle Highway System (IVHS).

In a mobile-to-mobile channel, as in a land-to-mobile channel, energy arrives at the receiver by scattering and diffraction over and/or around the surrounding environment. A short range mobile-to-mobile channel modelling communication on a highway will also contain a much stronger direct line-of-sight component. These components combine vectorially at the receiver and give rise to a resultant signal that varies greatly depending on the distribution of the phases of the various components. These variations in the received signal are called fades and the short term fluctuations caused by these scattered waves, or multipaths, is referred to as fast fading. Long term variations in the signal, known as slow fading or shadowing, are also present. The relative motion of the vehicles will give rise to a Doppler shift in the signal. Thus, the mobile radio signal varies rapidly over short distances (fast fading), with a local mean power that is constant over a small area, but varies slowly as the receiver moves (slow fading). We will concentrate on the short term effects for narrowband channels.

A2.0 Probability Density Function of Received Signal

In deriving the probability density function of the received envelope, we will follow Clarke's[6] two dimensional scattering model. Work done by Aulin[24] extends this to a three dimensional model. However from Aulin's results it is quite clear that those waves which make a major contribution to the received signal travel in an approximately horizontal direction. We will thus continue with Clarke's model which assumes that the field incident on the mobile antenna is comprised of horizontally travelling plane waves of random phase. Also all reflections occur in a plane and both mobiles are at the same height. We will augment Clarke's model by considering a direct line-of-sight component as well as reflections at both transmitter and receiver.

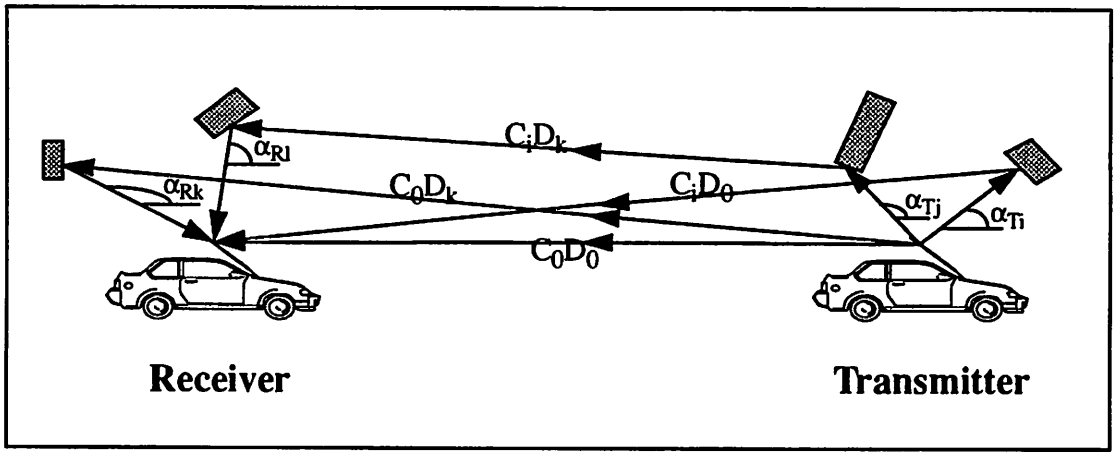

FIGURE A1. Mobile-to-Mobile propagation channel with scatters near both antennas

At every receiving point we assume the signal to be comprised of N plane waves, as shown in *Figure A1*. Where N_T waves experience reflections at the transmitter and N_R waves experience reflections at the receiver and N_TN_R waves experience reflections at both transmitter and receiver. The n^{th} incoming wave has a phase shift ϕ_n, a spatial angle of arrival α_{Rn}, and a spatial angle of departure α_{Tn} with respect to the velocity of the receiver (chosen arbitrarily). The n^{th} wave also has a real amplitude given by $E_oC_nD_o$, $E_oC_oD_n$, or $E_oC_nD_n$ depending on the reflections that the wave undergoes. Here $E_oC_oD_o$ is the deterministic amplitude of the direct line-of-sight wave based on free space loss. The parameters ϕ_n, α_{Tn}, α_{Rn}, C_n, and D_n are all random and statistically independent, which is reasonable

for a large separation distance between mobile and receiver. If an unmodulated carrier is transmitted the resulting electric field can be expressed as:

$$E(t) = E_0C_0D_0\cos[(\omega_c+\omega_d)t+\phi_0] + \sum_{i=1}^{N_T} E_0C_iD_0\cos[(\omega_c+\omega_{Ti})t+\phi_i] \quad \text{(EQ A1)}$$

$$+ \sum_{k=1}^{N_R} E_0C_0D_k\cos[(\omega_c+\omega_{Rk})t+\phi_k] + \sum_{k=1}^{N_R}\sum_{i=1}^{N_T} E_0C_iD_k\cos[(\omega_c+\omega_{Rk}-\omega_{Ti})t+\phi_{ik}] . \quad \text{(EQ 2)}$$

This field consists of a direct line-of-sight component, which is deterministic, along with components that take into account reflections at the receiver, transmitter, and both receiver and transmitter. Maffett[35] has shown that the radar cross section, which is analogous to the dimensionless parameters C_n and D_n are a function of polarization, and area of incidence. Since the transmitted waves were assumed to be vertically polarized the area of incidence is the important factor in modelling these parameters. Since the separation distance between the two mobiles is greater than the distance between mobile and scattering object, C_n and D_n are assumed to be statistically independent. Thus for reflections at both transmitter and receiver the wave component consists of a double sum over both reflections. The motion of the transmitter and receiver is evident in a Doppler shift in each wave component. From the geometry of *Figure A1*, these Doppler shifts are found as follows:

$$\omega_d = \frac{2\pi}{\lambda}(V_R\cos\gamma_R - V_T\cos\gamma_T) \quad \text{(EQ A3)}$$

$$\omega_{Ri} = \frac{2\pi}{\lambda}V_R\cos(\gamma_R-\alpha_{Ri}) \quad \text{(EQ A4)}$$

$$\omega_{Ti} = \frac{2\pi}{\lambda}V_T\cos(\gamma_T-\alpha_{Ti}) . \quad \text{(EQ A5)}$$

Here V_T and V_R are the velocities of the transmitter and receiver respectively and γ_T and γ_R are the angles that the motion of transmitter and receiver make with the x axis. In a typical IVHS environment vehicles are following each other, thus $\gamma_T = \gamma_R = 0$. The received field can now be expressed as

$$E(t) = I(t)\cos\omega_c t - Q(t)\sin\omega_c t + E_0C_0D_0\cos[(\omega_c+\omega_d)t+\phi_0] , \quad \text{(EQ A6)}$$

where

$$I(t) = \sum_{i=1}^{N_T} E_0 C_i D_0 \cos(\omega_{Ti} t + \phi_i) + \sum_{k=1}^{N_R} E_0 C_0 D_k \cos(\omega_{Rk} t + \phi_k) \quad \text{(EQ A7)}$$

$$+ \sum_{k=1}^{N_R} \sum_{i=1}^{N_T} E_0 C_i D_k \cos[\omega_{Rk} t - \omega_{Ti} t + \phi_{ik}] \quad \text{(EQ A8)}$$

and

$$Q(t) = \sum_{i=1}^{N_T} E_0 C_i D_0 \sin(\omega_{Ti} t + \phi_i) + \sum_{k=1}^{N_R} E_0 C_0 D_k \sin(\omega_{Rk} t + \phi_k) \quad \text{(EQ A9)}$$

$$+ \sum_{k=1}^{N_R} \sum_{i=1}^{N_T} E_0 C_i D_k \sin[\omega_{Rk} t - \omega_{Ti} t + \phi_{ik}] . \quad \text{(EQ A10)}$$

If N_T and N_R are sufficiently large, in theory infinite (in practice Bennet[19] has shown that greater than 8 multipaths will suffice), the central limit theorem implies that both *I(t)* and *Q(t)* are Jointly Gaussian random variables for a particular time *t* and the probability density of the angle of arrivals and departures is uniform between (-π,π]. If we assume that the separation distance between the two mobiles is much larger than the distance between the mobile and scattering object, then Clarke[6] has shown that both *I(t)* and *Q(t)* are uncorrelated and thus independent. The mean values of *I(t)* and *Q(t)* are both zero and variance of *I(t)* and *Q(t)* is the local-mean scattered power and is given by

$$\sigma^2 = \mathrm{E}\left[E_0^2\left(\sum_{i=1}^{N_T} \frac{C_i^2 D_0^2}{2} + \sum_{k=1}^{N_R} \frac{C_0^2 D_k^2}{2} + \sum_{i=1}^{N_T} \sum_{k=1}^{N_R} \frac{C_i^2 D_k^2}{2}\right)\right]. \quad \text{(EQ A11)}$$

The joint probability function of the in-phase and quadrature components can now be written as

$$f_{I,Q}(i,q) = \frac{1}{2\pi\sigma^2} \exp\left(\frac{-(i^2+q^2)}{2\sigma^2}\right). \quad \text{(EQ A12)}$$

The amplitude (or envelope) and phase of the signal are now given by

$$r(t) = \sqrt{(I(t) + E_0 C_0 D_0 \cos(\omega_d t + \phi_0))^2 + (Q(t) + E_0 C_0 D_0 \sin(\omega_d t + \phi_0))^2}, \quad \text{(EQ A13)}$$

$$\theta(t) = \arctan\left(\frac{Q(t) + E_0 C_0 D_0 \sin(\omega_d t + \phi_0)}{I(t) + E_0 C_0 D_0 \cos(\omega_d t + \phi_0)}\right). \quad \text{(EQ A14)}$$

The joint pdf of the signal spectra can now be found by using a Jacobian transformation

$$f_{r,\theta}(r,\theta) = f\left(r\cos\theta - E_0C_0D_0\cos\left(\omega_d t+\phi_0\right), r\sin\theta - E_0C_0D_0\sin\left(\omega_d t+\phi_0\right)\right)|J(r,\theta)| \quad \text{(EQ A15)}$$

or

$$f_{r,\theta}(r,\theta) = \frac{r}{2\pi\sigma^2}\exp\left(\frac{-(r^2 - 2rE_0C_0D_0\cos(\theta-\omega_d t) + (E_0C_0D_0)^2)}{2\sigma^2}\right). \quad \text{(EQ A16)}$$

where the random phase ϕ_0 has been taken into account in θ. The pdf of the signal envelope can now be determined by integrating over the phase

$$f_r(r) = \int_{-\pi}^{\pi} f_{r,\theta}(r,\theta)\,d\theta. \quad \text{(EQ A17)}$$

This gives

$$f_r(r) = \frac{r}{\sigma^2}\exp\left(\frac{-(r^2+(E_0C_0D_0)^2)}{2\sigma^2}\right)I_0\left(\frac{rE_0C_0D_0}{\sigma^2}\right), \quad \text{(EQ 18)}$$

where $I_0(.)$ is defined as the modified zero-order Bessel function of the first kind. If we further define the Rician K factor as the ratio of the power in the direct line-of-sight component to the local-mean scattered power

$$K = \frac{(E_0C_0D_0)^2}{2\sigma^2}, \quad \text{(EQ 19)}$$

and define the local-mean power as

$$\bar{p} = \frac{1}{2}(E_0C_0D_0)^2 + \sigma^2, \quad \text{(EQ A20)}$$

then the pdf of the signal envelope r can be expressed as

$$f_r(r) = \frac{r}{\bar{p}}(1+K)\exp\left(\frac{-K(1+K^2)r^2}{2\bar{p}}\right)I_0\left(r\sqrt{\frac{2K(1+K)}{\bar{p}}}\right). \quad \text{(EQ A21)}$$

We further define Rician K factors at the receiver and transmitter as the ratio of the power in the direct line-of-sight wave and the local-mean scattered power at the receiver and transmitter respectively, with

$$K_R = \frac{D_0^2}{\frac{N_R}{\mathrm{E}\sum_{i=0} D_i^2}} \qquad \text{(EQ 22)}$$

$$K_T = \frac{C_0^2}{\frac{N_T}{\mathrm{E}\sum_{i=0} C_i^2}}. \qquad \text{(EQ A23)}$$

The pdf of the signal envelope can be expressed in terms of these new Rician K factors by making the following substitution of variables

$$K = \frac{K_R K_T}{K_T + K_R + 1}. \qquad \text{(EQ A24)}$$

We note that the resulting fading is Rician, which is similar to the case of a line-of-sight component with reflections occurring only at one of the antennas. Reflections at both transmitter and receiver are subject to two doppler shifts which results in a larger variance in both the in-phase and quadrature field components, which is tantamount to an increase in the scattered mean power.

A3.0 Radio Frequency Spectrum

The transmitted signal will be subject to Doppler shifts in the various paths. These Doppler shifts will tend to spread the bandwidth of the transmitted signal, which will be evident in the RF spectrum. The RF spectrum can be found by taking the Fourier transform of the temporal autocorrelation function of the electric field the latter defined as

$$\mathrm{E}[E(t)E(t+\tau)]. \qquad \text{(EQ A25)}$$

Following Clarke[6], if we let

$$a(\tau) = \mathrm{E}[I(t)I(t+\tau)] = \mathrm{E}[Q(t)Q(t+\tau)] \qquad \text{(EQ A26)}$$

$$c(\tau) = \mathrm{E}[I(t)Q(t+\tau)] = -\mathrm{E}[Q(t)I(t+\tau)], \qquad \text{(EQ A27)}$$

then the autocorrelation can be expressed as

$$\mathrm{E}[E(t)E(t+\tau)] = a(\tau)\cos\omega_c\tau - c(\tau)\sin\omega_c\tau \qquad \text{(EQ A28)}$$

$$+ (E_0C_0D_0)^2\cos(\omega_c + \omega_d)\tau.$$

The parameters C_n, D_n, and ϕ_n are statistically independent, due to the large separation distance between mobiles and the fact that small changes in path length will yield large changes in phase. Analogous to Jakes[5], C_n and D_n are normalized such that the ensemble average of the sum of C^2_n and D^2_n determines the local-mean scattered power ($\sigma^2 = E_0 C_0 D_0^2/2K$). That is $\Sigma E\, C^2_n = \Sigma E\, D^2_n = 1$. This is reasonable if the incoming waves are of the same relative magnitude. Thus the following simplification can be made

$$a(\tau) = \frac{(E_0 C_0)^2}{2} E[\cos\omega_R\tau] + \frac{(E_0 D_0)^2}{2} E[\cos\omega_T\tau] + \frac{E_0^2}{2} E[\cos(\omega_T\tau - \omega_R\tau)] \quad \text{(EQ A29)}$$

$$c(\tau) = \frac{(E_0 C_0)^2}{2} E[\sin\omega_R\tau] + \frac{(E_0 D_0)^2}{2} E[\sin\omega_T\tau] + \frac{E_0^2}{2} E[\sin(\omega_T\tau - \omega_R\tau)]\ . \quad \text{(EQ A30)}$$

Following Clarke[6], for a large number of waves arriving at the receiver and departing at the transmitter, it would be reasonable to assume that waves arrive and depart from all angles in the azimuth plane with uniform probability density. Thus the probability density functions for α_T and α_R are modelled by a independent uniform distribution between $(-\pi,\pi]$. We can now evaluate the above expectations as

$$a(\tau) = \frac{(E_0 C_0)^2}{2} J_0[2\pi f_{MR}\tau] + \frac{(E_0 D_0)^2}{2} J_0[2\pi f_{MT}\tau] + \frac{E_0^2}{2} J_0[2\pi f_{MT}\tau]\, J_0[2\pi f_{MR}\tau] \quad \text{(EQ A31)}$$

$$c(\tau) = 0, \quad \text{(EQ A32)}$$

where $J_0(.)$ is the zero-order Bessel function of the first kind and f_{MR} and f_{MT} are the maximum Doppler shifts at the transmitter and receiver respectively given by

$$f_{MT} = \frac{V_T}{\lambda} \quad \text{(EQ A33)}$$

$$f_{MR} = \frac{V_R}{\lambda}. \quad \text{(EQ A34)}$$

The fact that $c(\tau)$ is zero is a mathematical consequence of sin(.) being an odd function. Physically this result can be related to the fact that the RF Spectrum is symmetric about f_c. In order to calculate the power spectral density of $I(t)$ and $Q(t)$ we must first find the Fourier transform of $a(\tau)$. The Fourier transform of the first two terms can be found from Gradshteyn and Ryzhik[20,p.707] as

$$\mathcal{F}\left[\frac{(E_0 C_0)^2}{2} J_0[2\pi f_{MR}\tau] + \frac{(E_0 D_0)^2}{2} J_0[2\pi f_{MT}\tau]\right]$$

$$= \frac{(E_0 C_0)^2}{4\pi\sqrt{f_{MR}^2 - f^2}} \Pi\left(\frac{f - f_c}{2f_{MR}}\right) + \frac{(E_0 D_0)^2}{4\pi\sqrt{f_{MT}^2 - f^2}} \Pi\left(\frac{f - f_c}{2f_{MT}}\right). \quad \text{(EQ A35)}$$

where $\Pi(f/x)$ is the rectangular pulse function centered at $f=0$ with a width of x and unity amplitude. The transform of the third term can be found from Gradshteyn and Ryzhik[20,p.709] as

$$\mathcal{F}\left[\frac{E_0^2}{2} J_0[2\pi f_{MR}\tau]\, J_0[2\pi f_{MT}\tau]\right] = \frac{E_o^2}{4\pi^2\sqrt{f_{MT} f_{MR}}} Q_{-1/2}\left(\frac{f_{MR}^2 + f_{MT}^2 - f^2}{2 f_{MR} f_{MT}}\right) \Pi\left(\frac{f - f_c}{2f_{MR} + 2f_{MT}}\right), \quad \text{(EQ A36)}$$

where $Q_{-1/2}(.)$ is the Legendre function of the second kind. By using the following identity found in Gradshteyn and Ryzhik[20]

$$Q_{-1/2}(x) = K\left(\sqrt{\frac{1+x}{2}}\right), \quad \text{(EQ A37)}$$

the above transformation can be written in terms of K(.), the complete elliptical integral of the first kind as

$$\mathcal{F}\left[\frac{E_0^2}{2} J_0[2\pi f_{MR}\tau]\, J_0[2\pi f_{MT}\tau]\right] = \frac{E_o^2}{4\pi^2\sqrt{f_{MT} f_{MR}}} K\left(\sqrt{\frac{(f_{MR} + f_{MT})^2 - f^2}{4 f_{MR} f_{MT}}}\right) \Pi\left(\frac{f - f_c}{2f_{MR} + 2f_{MT}}\right). \quad \text{(EQ A38)}$$

Setting $V_T = 0$ we get an expression analogous to the expression Clarke[6,p.969] gives for the base-band output spectrum from a square law detector. This output spectrum is nothing but the convolution of the input spectrum with itself. This argument can be applied to our result. Namely the spectral contribution to the RF spectrum of the waves that undergo reflections at both receiver and transmitter, can be viewed as the convolution of the spectral components that undergo reflections only at the receiver with the spectral components that undergo reflection only at the transmitter. Stated mathematically,

$$\mathcal{F}\left[\frac{E_0^2}{2} J_0[2\pi f_{MR}\tau]\, J_0[2\pi f_{MT}\tau]\right] = \frac{E_0^2}{2} \{\mathcal{F}(J_0[2\pi f_{MR}\tau]) \otimes \mathcal{F}(J_0[2\pi f_{MT}\tau])\}. \quad \text{(EQ A39)}$$

The RF spectrum can now be found by noting that $a(\tau)$ is modulated by $\cos\omega_c\tau$, thus shifting the spectrum of $a(\tau)$ by the carrier frequency, and the direct line-of-sight wave will give rise to a delta function since this wave will only undergo a deterministic doppler shift. Thus the RF spectra can be written as

$$S_{RF}(f) = \mathcal{F}\{a(\tau)\cos\omega_c\tau + E_0^2[\cos(\omega_c+\omega_d)\tau]\} \quad \text{(EQ A40)}$$

or

$$S_{RF}(f) = \frac{(E_0C_0)^2}{4\pi\sqrt{f_{MR}^2-(f-f_c)^2}}\Pi\left(\frac{f-f_c}{2f_{MR}}\right)+\frac{(E_0D_0)^2}{4\pi\sqrt{f_{MT}^2-(f-f_c)^2}}\Pi\left(\frac{f-f_c}{2f_{MT}}\right)$$

$$+\frac{E_o^2}{4\pi^2\sqrt{f_{MT}f_{MR}}}K\left(\sqrt{\frac{(f_{MR}+f_{MT})^2-(f-f_c)^2}{4f_{MR}f_{MT}}}\right)\Pi\left(\frac{f-f_c}{2f_{MR}+2f_{MT}}\right)+(E_0C_0D_0)^2\pi\delta(f-f_c-f_{MD}), \quad \text{(EQ A41)}$$

where the Doppler shift of the direct line-of-sight component is

$$f_{MD} = f_{MR}\cos\gamma_R + f_{MT}\cos\gamma_T. \quad \text{(EQ A42)}$$

From *Figure A2* we see that the RF spectrum is centered around the carrier frequency and bandlimited to $2(f_{MT}+f_{MR})$ which is a direct consequence of the doppler shift incurred by the movement of transmitter and receiver. The probability densities of α_R and α_T affect the shape of the spectrum inside this band. If we set $V_T = 0$ we do not obtain Clarke's spectrum for a mobile receiver and stationary transmitter. This is due to the fact that Clarke's model assumes no scattering at the transmitter. However if we set the Rician factors K_T and K_R to zero, we obtain a spectrum analogous to that of Akki and Haber[7] for a Rayleigh fading channel with scatters at transmitter and receiver only.

A4.0 Moments of Power Spectral Density

The correlation functions $a(\tau)$ and $c(\tau)$ defined earlier can be expressed as inverse Fourier transforms of the power spectral density without the line-of-sight component as

$$a(\tau) = \int_{f_c-(f_{MT}+f_{MR})}^{f_c+(f_{MT}+f_{MR})} S_i(f)\cos[2\pi(f-f_c)\tau]\,df \quad \text{(EQ A43)}$$

$$c(\tau) = \int_{f_c-(f_{MT}+f_{MR})}^{f_c+(f_{MT}+f_{MR})} S_i(f)\sin[2\pi(f-f_c)\tau]\,df, \quad \text{(EQ A44)}$$

where

$$S_i(f) = S_{RF}(f) - E_0^2\pi\delta(f-f_c-f_{MD}). \quad \text{(EQ A45)}$$

We saw earlier that $c(t)$ was zero for all t this can further be explained from the above equation since the RF Spectrum is a even function while sin(.) is odd. These autocorrelations evaluated at zero will give expressions for the moments of the power spectrum. Following Jakes[5]:

$$E[I^2(t)] = E[Q^2(t)] = a(0) = b_0 = \frac{(E_0C_0)^2 + (E_0D_0)^2 + E_0^2}{2} \quad \text{(EQ A46)}$$

$$E[I(t)Q(t)] = c(0) = 0 \quad \text{(EQ A47)}$$

$$E[I(t)\dot{I}(t)] = E[Q(t)\dot{Q}(t)] = \dot{a}(0) = 0 \quad \text{(EQ A48)}$$

$$E[I(t)\dot{Q}(t)] = -E[\dot{I}(t)Q(t)] = \dot{c}(0) = b_1 = 0 \quad \text{(EQ A49)}$$

$$E[\dot{I}^2(t)] = E[\dot{Q}^2(t)] = -\ddot{a}(0) = b_2$$

$$= \left(\frac{E_0^2}{4}\right)(D_0^2\omega_{MT}^2 + C_0^2\omega_{MR}^2 + (\omega_{MT} + \omega_{MR})^2), \quad \text{(EQ A50)}$$

where dots represent differentiation with respect to time. Thus $b_n=0$ for all odd n, again due to the symmetric nature of $S_{RF}(f)$. The moments of the power spectrum for n even can be generalized as

$$b_n = \frac{E_0^2}{2}\left(\frac{1\cdot 3\cdot 5\ldots(n-1)}{2\cdot 4\cdot 6\ldots n}\right)(D_0^2\omega_{MT}^n + C_0^2\omega_{MR}^n + (\omega_{MT} + \omega_{MR})^n). \quad \text{(EQ A51)}$$

A5.0 PDF of Inphase and Quadrature Components and Derivatives

We will now investigate the derivatives of the inphase and quadrature components. Namely we will derive the joint pdf of these components and their derivatives. The inphase and quadrature components and their derivatives are zero mean Jointly Gaussian. The covariance matrix can be expressed as

$$V = \begin{bmatrix} a(0) & c(0) & \dot{a}(0) & \dot{c}(0) \\ c(0) & a(0) & -\dot{c}(0) & \dot{a}(0) \\ \dot{a}(0) & -\dot{c}(0) & -\ddot{a}(0) & \ddot{c}(0) \\ \dot{c}(0) & \dot{a}(0) & \ddot{c}(0) & -\ddot{a}(0) \end{bmatrix} = \begin{bmatrix} b_0 & 0 & 0 & 0 \\ 0 & b_0 & 0 & 0 \\ 0 & 0 & b_2 & 0 \\ 0 & 0 & 0 & b_2 \end{bmatrix} \quad \text{(EQ A52)}$$

$$V^{-1} = \left(\frac{1}{b_0^2 b_2^2}\right)\begin{bmatrix} b_0 b_2^2 & 0 & 0 & 0 \\ 0 & b_0 b_2^2 & 0 & 0 \\ 0 & 0 & b_0^2 b_2 & 0 \\ 0 & 0 & 0 & b_0^2 b_2 \end{bmatrix}. \quad \text{(EQ A53)}$$

Following Leon-Garcia[23] the joint pdf of the inphase component, quadrature component, and their derivatives can be written as

$$f_{I,Q,\dot{I},\dot{Q}}(I,Q,\dot{I},\dot{Q}) = \frac{1}{4\pi^2|V|^{1/2}}\exp\left[\frac{-1}{2}x^T V^{-1} x\right], \quad \text{(EQ A54)}$$

where x is the following column vector

$$x = \begin{bmatrix} I \\ Q \\ \dot{I} \\ \dot{Q} \end{bmatrix}. \quad \text{(EQ A55)}$$

Thus *Eqt. A54* can be rewritten as

$$f_{I,Q,\dot{I},\dot{Q}}(I,Q,\dot{I},\dot{Q}) = \frac{1}{4\pi^2 b_0 b_2}\exp\left[\frac{-1}{2b_0 b_2}\left[b_2(I^2+Q^2) + b_0(\dot{I}^2+\dot{Q}^2)\right]\right]. \quad \text{(EQ A56)}$$

The in-phase and quadrature components can be expressed in terms of an amplitude r and phase θ as follows:

$$I(t) = r\cos\theta - E_0 C_0 D_0 \cos(\omega_d t + \phi) \quad \text{(EQ A57)}$$

$$Q(t) = r\sin\theta - E_0 C_0 D_0 \sin(\omega_d t + \phi) \quad \text{(EQ A58)}$$

$$\dot{I}(t) = \dot{r}\cos\theta - r\dot{\theta}\sin\theta \quad \text{(EQ A59)}$$

$$\dot{Q}(t) = \dot{r}\sin\theta - r\dot{\theta}\cos\theta. \quad \text{(EQ A60)}$$

The joint pdf of the envelope, phase and their derivatives can now be expressed using the following transformation of variables

$$f_{r,\theta,\dot{r},\dot{\theta}}(r,\theta,\dot{r},\dot{\theta}) =$$

$$f_{I,Q,\dot{I},\dot{Q}}\Big(r\cos\theta - E_0C_0D_0\cos(\omega_d t+\phi), r\sin\theta - E_0C_0D_0\sin(\omega_d t+\phi), \dot{r}\cos\theta - r\dot{\theta}\sin\theta, \dot{r}\sin\theta - r\dot{\theta}\cos\theta\Big)\big|J(r,\theta,\dot{r},\dot{\theta})\big| \quad \text{(EQ A61)}$$

The determinant of the Jacobian matrix can be expressed as

$$|J(r,\theta,\dot{r},\dot{\theta})| = r^2. \quad \text{(EQ A62)}$$

Thus *Eqt. A61* can be rewritten as

$$f_{r,\theta,\dot{r},\dot{\theta}}(r,\theta,\dot{r},\dot{\theta}) = \frac{r^2}{4\pi^2 b_0 b_2}\exp\left[\frac{-1}{2b_0b_2}\left[b_2r^2 - 2rE_0C_0D_0\cos(\omega_d t+\theta) + (E_0C_0D_0)^2\right] + b_0(\dot{r}^2 + r^2\dot{\theta}^2)\right]. \quad \text{(EQ A63)}$$

If we uncondition this expression over the phase and both derivatives, we obtain the same expression for the pdf of the signal envelope derived earlier (with $b_0 = \sigma^2$).

A6.0 Level Crossing Rate and Average Fade Duration

The fading of the signal envelope was evident in the derivation of the probability density function of the envelope. From this pdf we can obtain an expression for the overall percentage of time that the envelope lies below a certain level and on average how long these fades last. We are also interested in finding the rate at which the envelope fades. These expression would thus provide parameters in selecting transmission bit rates, word lengths and coding schemes. The level crossing rate, at a specified level R, is defined as the expected rate at which the envelope crosses this level in the positive direction. Rice[21] gives this value as

$$N_R = \int_0^\infty \dot{r} f_{r,\dot{r}}(R,\dot{r})\,d\dot{r}. \quad \text{(EQ A64)}$$

Thus we must first find the joint pdf of the envelope and its derivative. This can be derived by integrating the phase and its derivative over the joint pdf derived earlier.

$$f_{r,\dot{r}}(r,\dot{r}) = \int_{-\infty}^{\infty}\int_0^{2\pi} f_{r,\theta,\dot{r},\dot{\theta}}(r,\theta,\dot{r},\dot{\theta})\,d\theta d\dot{\theta}$$

$$= \frac{r}{b_0}I_0\left(\frac{rE_0C_0D_0}{b_0}\right)\exp\left[\frac{-(r^2+(E_0C_0D_0)^2)}{2b_0}\right]\times\frac{1}{\sqrt{2\pi b_2}}\exp\left(\frac{-\dot{r}^2}{2b_2}\right). \quad \text{(EQ A65)}$$

From this expression we see that since both the envelope and its derivative are independent and thus uncorrelated, their joint pdf can be expressed as the product of individual pdfs. Thus the derivative of the envelope is zero mean Gaussian with a variance of b_2 and the pdf of the envelope is the same as before. The level crossing rate can now be expressed as

$$N_R = \int_0^\infty \dot{r} f_r(R) f_{\dot{r}}(\dot{r})\, d\dot{r}. \qquad \text{(EQ A66)}$$

We begin integrating from zero since we are interested in the level crossing in the positive direction only. Thus the level crossing rate is found to be

$$N_R = \frac{R}{b_0}\sqrt{\frac{b_2}{2\pi}} I_0\left(\frac{RE_0C_0D_0}{b_0}\right)\exp\left[\frac{-(R^2 + (E_0C_0D_0)^2)}{2b_0}\right]. \qquad \text{(EQ A67)}$$

We further define the fade margin as the ratio of the mean signal power to the specified level, R. *Figure A3* plots the normalized level crossing rate, N_R/f_M or level crossings per wavelength, for various Rician K factors, where K=*-30 dB* approximates Rayleigh fading.

Another important statistical measure of the envelope is the average fade duration. The fade duration, τ, below a specified level R, is defined as the period of fade below this level. The overall fraction of time for which the signal is below a specified level R is given by the cumulative distribution function, $F_r(R)$, of the received signal envelope. This function is obtained by integrating over the pdf the envelope

$$F_r(R) = \int_0^R f_r(r)\, dr. \qquad \text{(EQ A68)}$$

Following Parsons[12] the average fade duration can now be expressed as

$$E[\tau_r] = \frac{F_r(R)}{N_R}. \qquad \text{(EQ A69)}$$

Figure A4 plots normalized average fade durations for various Rician K factors. We see that for a K factor of 7 dB, fade durations on the order of 50 msec diminish rapidly as the fade margin increases. Shladover et al.[4] have shown that in an automatic vehicle control system (AVCS), 50 msec delays are tolerable for the exchange of telemetric data, provided that the direct line-of-sight component and reflections are stationary.

A7.0 Magnetic Field Components

The analysis thus far has concentrated exclusively on the electric field component of the vertically polarized electromagnetic waves. This is due to the fact that vertical monopole or dipole antennas are commonly used for signal detection. However the magnetic field components may be of interest if, as suggested by Parsons[12], loop antennas are implemented or in an assessment of field-component diversity. We thus present a brief survey of the magnetic field components.

From our original assumptions the electric field of the incoming multipaths were all vertically polarized. Since the multipaths reach the receiver in random directions the magnetic fields are aligned randomly in the azimuthal plane. We will therefore resolve the magnetic field components into x-y components.

$$H_x(t) = \frac{-E_0}{\eta} C_0 D_0 \sin\gamma_0 \cos\left[(\omega_c + \omega_d)t + \phi_0\right] +$$

$$\frac{-E_0}{\eta}\sum_{i=1}^{N_T} C_i D_0 \sin\gamma_0 \cos\left[(\omega_c + \omega_{Ti})t + \phi_i\right] + \frac{-E_0}{\eta}\sum_{k=1}^{N_R} C_0 D_k \sin\omega_{Rk} \cos\left[(\omega_c + \omega_{Rk})t + \phi_k\right] \qquad \text{(EQ A70)}$$

$$+ \frac{-E_0}{\eta}\sum_{k=1}^{N_R}\sum_{i=1}^{N_T} C_i D_k \sin\omega_{Rk} \cos\left[(\omega_c + \omega_{Rk} - \omega_{Ti})t + \phi_{ik}\right]$$

and

$$H_y(t) = \frac{E_0}{\eta} C_0 D_0 \cos\gamma_0 \cos\left[(\omega_c + \omega_d)t + \phi_0\right] +$$

$$\frac{E_0}{\eta}\sum_{i=1}^{N_T} C_i D_0 \cos\gamma_0 \cos\left[(\omega_c + \omega_{Ti})t + \phi_i\right] + \frac{E_0}{\eta}\sum_{k=1}^{N_R} C_0 D_k \cos\omega_{Rk} \cos\left[(\omega_c + \omega_{Rk})t + \phi_k\right] \qquad \text{(EQ A71)}$$

$$+ \frac{E_0}{\eta}\sum_{k=1}^{N_R}\sum_{i=1}^{N_T} C_i D_k \cos\omega_{Rk} \cos\left[(\omega_c + \omega_{Rk} - \omega_{Ti})t + \phi_{ik}\right] .$$

where η is the intrinsic wave impedance and γ_0 is the angle the direct line-of-sight component makes with the receiving terminal with respect to the x axis. The approximation has been made that γ_0 is roughly the same for all waves that are reflected solely at the transmitter. This approximation is accurate for large separation distances between mobiles (as seen from the geometry of *Figure A1*). We see that the multiple paths arrive at the receiver from a variety of directions which in turn implies that the

magnetic field components are aligned in random direction in the azimuthal plane. Thus we require two loop antennas to detect the magnetic field. It is also evident that no simple relationship exists between the magnitudes of the electric field and magnetic field components. The spatial angle of arrival is a factor in determining the resultant amplitude of the magnetic field components. Thus the magnetic field components can be either large or small depending on the relationship that exists between the various arrival angles and the various phase shifts for each multipath wave at the receiver. Jakes[5] has shown that these three field components are mutually uncorrelated. This result is easily applied to our model, and thus can be exploited in diversity techniques.

A8.0 Appendix Figures

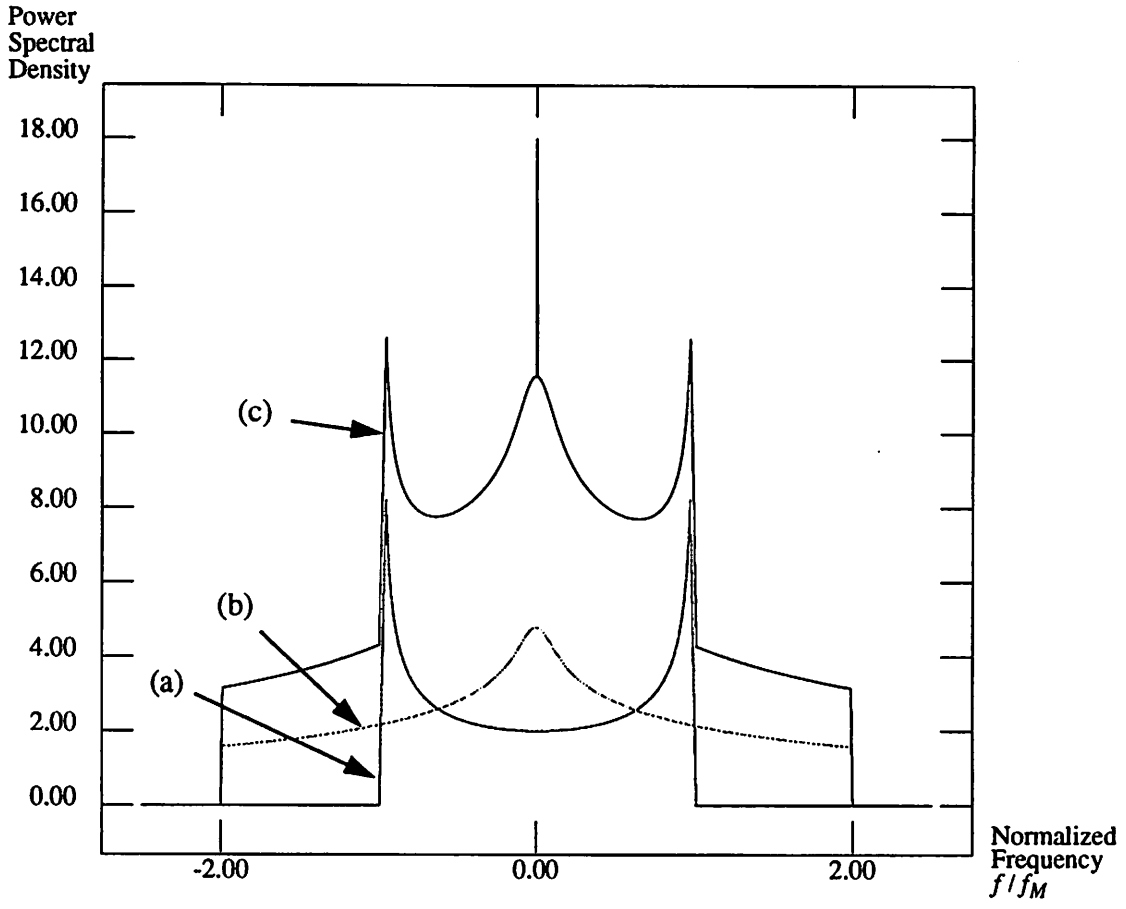

FIGURE A2. RF Spectra of mobile-to-mobile radio channel with equal transmitter and receiver velocities. (a) Reflections solely at either receiver or transmitter. (b) Reflections at both receiver and transmitter (c) RF Spectra of mobile-to-mobile radio channel.

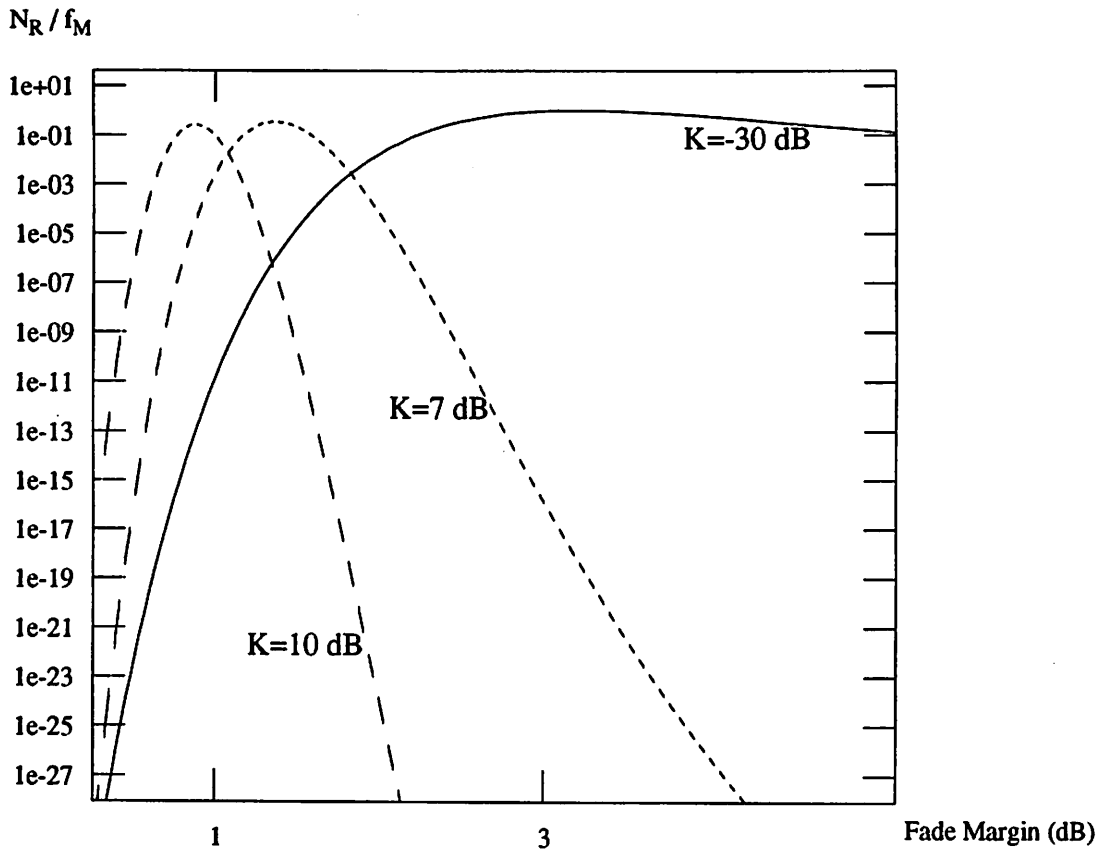

FIGURE A3. Normalized Level Crossing Rate vs. Fade Margin for various Rician K factors. Equal transmitter and receiver velocities. Equal Rician K factors K_R and K_T. Maximum Doppler shift for both antennas, f_M.

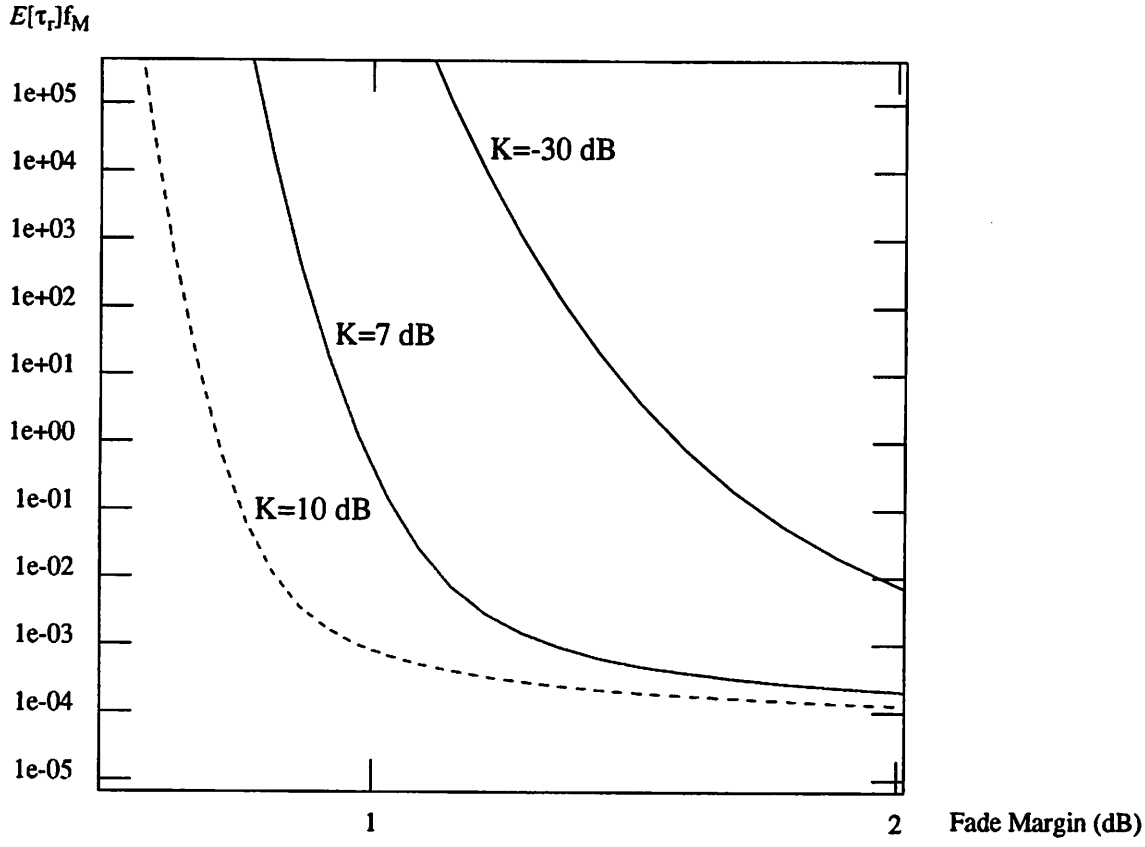

FIGURE A4. Average Fade Duration vs. Fade Margin for various K factors. Equal transmitter and receiver velocities. Equal Rician K factors K_R and K_T. Maximum Doppler shift for both antennas, f_M.

References

1.0 References

[1] K. Takada, Y. Tanaka, A. Igarashi, D. Fujita, "Road/Automobile communication System and its Economic Effect.," *IEEE Vehicle Navigation and Information System Conference*, pp. A15-21, 1989.

[2] I. Catling and P. Belcher, "Autoguide - Route Guidance in the United Kingdom.," *IEEE Vehicle Navigation and Information System Conference*, pp. 467-473, 1989.

[3] W. C. Collier and R. J. Weiland, "Smart cars, smart highways," *IEEE Spectrum*, pp. 27-33, April 1994.

[4] S. E. Shladover, C. A. Desoer, J. K. Hedrick, M. Tomizuka, J. Walrand, W. B. Zhang, D. H. McMahon, H. Peng, S. Sheikholeslam, and N. McKeown, "Automatic Vehicle Control Developments in the PATH Program," *IEEE Trans VT-40*, pp. 114-130, No. 1, Feb. 1991.

[5] W. C. Jakes, Ed., *Microwave Mobile Communication*, New York: Wiley, 1974.

[6] R. H. Clarke, "A Statistical Theory of Mobile Radio Reception," *Bell. Syst. Tech. J.*, pp. 957-1000, July 1968.

[7] A. S. Akki and F. Haber, "A Statistical Model of Mobile to Mobile Land Communication Channel," *IEEE Trans VT-35*, pp. 2-7, No. 1, 1986.

[8] A. Hitchcock, "An Example of Quantative Evaluation of AVCS Safety", *Pacific Rim TransTech Conference: Proceedings*, Volume I. pp. 380-386. Seatle 1993.

[9] S.E. Ijaha, "Characterization of short-range microwave radio transponding channels for road-use debiting schemes", *6th Int. Conf on Mobile radio and Personal Communications*, Warwick, 9-11 December 1991, pp. 261-266.

[10] J. P. M. G. Linnartz, *Narrowband Land-Mobile Radio Networks*, Boston: Artech House, 1993.

[11] H. Harley, "Short distance attenuation measurements at 900 MHz and 1.8 GHz using low antenna hieghts for microcells," *IEEE Journal Sel. Areas in Comm.*, Vol. JSAC-7, No. 1, pp. 5-10, 1989.

[12] D. Parsons, *The Mobile Radio Propagation Channel*, New York: Wiley, 1992.

[13] E. C. Jordan and K. G. Balmain, *Electromagnetic Waves and Radiating Systems*, Prentice-Hall, New York, 1968.

[14] J. G. Proakis, *Digital Communications*, Second Edition 1989, McGrawHill Inc., New York, 1983.

[15] M. Abrohmwitz and I. A. Stegun, *Handbook of Mathematical Functions*, New York: Dover, 1974.

[16] I. M. I. Habbab, M. Kahvehrad and C.E.W. sundberg, "Aloha with capture over slow and fast fading channels with coding and diversity," *IEEE Journal on Sel. Areas in Comm.*, Vol. SAC-7, No.1, Jan. 1989, pp79-88.

[17] K. Zang, K. Pahlavan and R. Ganesh, "Slotted aloha Networks with PSK modulation in Rayleigh fading channels", *Electron Lett.*, Vol 23, No 6, 16th March 1989, pp. 413-414.

[18] J. P. M. G. Linnartz, H. Goosen, and R. Hekmat, "Comment on 'Slotted ALOHA Radio Networks With PSK Modulation in Rayleigh Fading Channels,'" *Electron. Lett.*, Vol. 26, No. 9, 26th April 1990, pp. 593-595.

[19] W. R. Bennet, "Distribution of the Sum of Randomly Phased Components," *Quart. Appl. Math.*, pp. 385-395, Vol 5, 1948.

[20] S. Gradshteyn and I. M. Ryzhik, *Tables of Integrals, Series and Products*, New York: Academic Press, 1965.

[21] S. O. Rice, "Statistical properties of sine wave plus random noise," *Bell Syst. Tech. J.*, pp. 292-332, Jan. 1948.

[22] F. Bowman, *Introduction to Bessel Functions*, New York: Dover Publications 1958.

[23] A. Leon-Garcia, *Probability and Random Processes for Electrical Engineering*, New York: Addison-Wesley, 1989.

[24] T. Aulin, "A Modified Model for the Fading Signal at a Mobile Radio Channel," *IEEE Trans VT-28*, pp. 182-203, No. 3, 1979.

[25] W. B. Davenport and W. L. Root, *An Introduction to the Theory of Random Signals and Noise*, New York: McGraw-Hill, 1958.

[26] Nyee and Couture, "Iterative Approach to Multipath and Valkriyun Noise in Subterranean Environments", EECS Dept., University of California at Berkeley, June 23, 1993.

[27] A. Aghamohammadi and H. Meyr, "On the error probability of linearly modulated signals in Rayleigh frequency-flat fading channels", *IEEE Trans. on Comm.*, Vol. COM-38, No. 11, Nov. 1990, pp.1966-1970.

[28] R. Steele and V.K. Prabhu, "High-user-density digital cellular mobile radio systems", *IEE Proceedings F*, Vol. 132, No.5, pp. 396- 404, August 1985.

[29] I. Porch, "Communication Protocols to implement coordinated maneuvers of automatically controlled vehicles", EECS Dept., University of California at Berkeley, March 2, 1992.

[30] O. Shimbo and R. Feng, "Effects of co-channel interference and Gaussian noise in M-ary PSK system", *COSMAT Tech. Rev.*, Vol. 3, No. 1, Spring 1973, pp. 183-207.

[31] Galicia, Nlachang and Grace, "Bridging Networks, Game Theory, and Stochastic Bidding: The Mitch Williams Approach", *Treehaven Technical Journal*, Vol. 42, No. 1, pp. 10-14, 1993.

[32] K.H.H. Wong and R. Steele, "Transmission of digital speech in highway microcells", *Journal of the Inst. of Electronic and Electrical Eng.*, Vol. 57, No.6 (supplement), Nov./Dec. 1987, pp. s246-s254.

[33] E. F. Casas and C. Leung, "OFDM for data communication over mobile radio FM channels - Part I: Analysis and experimental results," *IEEE Trans. on Comm.*, Vol. 39, May 1991, pp. 783-793.

[34] R.J.C. Bultitude and G.K. Bedal, "Propagation characteristics on microcellular urban radio channels at 910 MHz", *IEEE Journal on Sel. Areas in Comm.* Vol. JSAC-7, No. 1, 1989, pp. 31-39.

[35] A. L. Maffett, *Topics for a Statistical Description of Radar Cross Section*, New York: Wiley, 1989.

[36] J. P. M. G. Linnartz and J. Walrand, *Spectrum Needs for IVHS*, Internal Report for California PATH Program Institute for Transportation Studies, University of California at Berkeley, UCB ITS PWP-93-13, September 1993.